PHYSICAL REVIEW C **92**, 014607 (2015)

Partial-wave analysis of $n + {}^{241}$Am reaction cross sections in the resonance region

G. Noguere and O. Bouland
CEA, DEN Cadarache, F-13108 Saint Paul Les Durance, France

S. Kopecky, C. Lampoudis, P. Schillebeeckx, and A. Plompen
EC-JRC-IRMM, B-2440 Geel, Belgium

F. Gunsing
CEA, DSM Saclay, F-91191 Gif-sur-Yvette, France

C. Sage
LPSC, Université Grenoble-Alpes, CNRS/IN2P3, F-38026 Grenoble, France

I. Sirakov
INRNE, BG-1784 Sofia, Bulgaria
(Received 17 April 2015; published 7 July 2015)

Cross sections for neutron-induced reactions of ^{241}Am in the resonance region have been evaluated. Results of time-of-flight cross section experiments carried out at the GELINA, LANSCE, ORELA and Saclay facilities have been combined with optical model calculations to derive consistent cross sections from the thermal energy region up to the continuum region. Resolved resonance parameters were derived from a resonance shape analysis of transmissions, capture yields, and fission yields in the energy region up to 150 eV using the REFIT code. From a statistical analysis of these parameters, a neutron strength function ($10^4 S_0 = 1.01 \pm 0.12$), mean level spacing ($D_0 = 0.60 \pm 0.01$ eV) and average radiation width ($\langle \Gamma_{\gamma_0} \rangle = 43.3 \pm 1.1$ meV) for s-wave resonances were obtained. Neutron strength functions for higher partial waves ($l > 0$) together with channel and effective scattering radii were deduced from calculations based on a complex mean-field optical model potential, applying an equivalent hard-sphere scattering radius approximation.

DOI: 10.1103/PhysRevC.92.014607 PACS number(s): 24.60.Dr, 25.40.Lw, 25.40.Ny, 25.60.Dz

I. INTRODUCTION

Studies of neutron-induced reaction cross sections of main importance for present and innovative nuclear reactor systems are part of a longstanding collaborative effort between the French Atomic Energy Commission (CEA) and Joint Research Centre of the European Commission (JRC-IRMM). In this work an evaluation of cross sections for neutron-induced reactions in ^{241}Am is described. The work is based on a resonance shape analysis of time-of-flight (TOF) cross section data and results from optical model calculations. To ensure a consistent description of the cross sections from the thermal energy region up to the continuum region, average resonance parameters were deduced from a combination of a statistical analysis of resolved parameters and results from optical model calculation.

In the resolved resonance range (RRR), parameters of individual s-wave resonances, i.e., resonance energies E_{λ_c} and partial widths ($\Gamma_{\lambda n_c}$, $\Gamma_{\lambda \gamma_c}$, $\Gamma_{\lambda f_c}$), were extracted from a resonance shape analysis of TOF cross section data. The resonance shape analysis code REFIT [1], based on the Reich-Moore approximation [2] of the R-matrix formalism [3], was used. In the least-squares adjustment, experimental data reported in the EXFOR library [4] together with results of recent capture and transmission experiments carried out by Lampoudis *et al.* [5] at the TOF facility of the JRC-IRMM were included. The resonance strengths and capture cross section at thermal energy reported in Ref. [5] are systematically higher (by more than 10%) compared to those recommended in international Evaluated Nuclear Data Files (JEFF, JENDL, ENDF/B). A similar systematic difference was observed in Ref. [5] when comparing the parameters of Lampoudis *et al.* with those resulting from capture measurements carried out at the LANSCE facility [6]. On the other hand a good agreement was found in Ref. [5] between the integral data calculated from the resonance parameters of Lampoudis *et al.* and those obtained from integral experiments carried out at the MELUSINE reactor located in Grenoble (France) [7,8]. An attempt was made to clarify the discrepancies between results derived from different TOF cross section data sets.

Like for ^{99}Tc [9], ^{127,129}I [10], and ^{237}Np [11] the neutron strength function S_0 and level spacing D_0 for s-wave neutrons were determined from a statistical analysis of resolved resonance parameters using the ESTIMA method [12]. This method also accounts for the contribution of missing levels. Neutron strength functions and scattering radii were derived from results of optical model calculations [13]. In the present work equivalent hard-sphere scattering radii are deduced from phase shifts originating from a complex mean-field coupled channel potential that was optimized for the nuclear system ^{241}Am $+ n$. The resulting average parameters were used to reconstruct the cross sections in the unresolved resonance region (URR) and to compare them with experimental data reported in the literature.

Similar procedures were already proposed by Moldauer [14] and more recently by Sirakov *et al.* [15]. The approach of Sirakov *et al.* was applied to analyze the unresolved resonance range of the ^{232}Th and ^{197}Au neutron cross sections [16,17].

II. NUCLEAR REACTION THEORY IN THE RESONANCE REGION

Nuclear reaction theories that are used to parametrize cross sections in the RRR and URR are briefly described. The division into two regions is due to experimental limitation. In the URR the time resolution of the TOF spectrometers is not sufficient to determine parameters of individual resonances and only allows average resonance parameters to be derived.

A. Resolved resonance formalism

Total and partial cross sections for neutron-induced reactions in the resolved resonance range can be expressed through the elements of the symmetric and unitary collision matrix U. For the total cross section, one obtains

$$\sigma_{tot_c}(E) = \frac{2\pi}{k^2} g_J (1 - \mathrm{Re}[U_c(E)]), \quad (1)$$

where $U_c(E) \equiv U_{cc}(E)$ is the diagonal collision matrix element for an entrance neutron channel $c = \{l,s,J\}$, k is the wave number of the incoming neutron in the center-of-mass system, and g_J is the statistical spin factor,

$$g_J = \frac{2J+1}{(2i+1)(2I+1)}, \quad (2)$$

with i, I, and J the spins of the neutron, target, and whole neutron-target system, respectively. The entrance channel is defined by the orbital angular momentum of the incoming neutron l, the total angular momentum J, and the channel spin s as a vectorial combination identical for both (I,i) and (l,J). For nonzero I (here $I = 5/2$) and nonzero l, the same total spin J may be obtained by either 1 or 2 different channel spins s. Due to splitting insensitivity, all neutron reaction widths or amplitudes are usually attributed to only one of the possible channel spins, called "'resonant," while the "non-resonant" one (if any) solely contributes in the phase shift. Thus, the conversion from an (l,s,J) into an (l,J) neutron channel formalism has generally been accepted in the resolved resonance range as considering only one independent neutron channel with a given (l,J) and providing an additional term in the potential scattering expression to include both channel-spin contributions [18].

The index of particle-pair identification α as part of the arbitrary channel representation α_c is sometimes omitted for the elastic neutron channel ($\alpha = n$), but is mandatory for the reaction ones, such as radiative capture ($\alpha = \gamma$) and fission ($\alpha = f$). In case of nonelastic channels the index $c = (l,J)$ determines the total spin and parity J^π conserved in the reaction, while for the elastic channels, l is also assumed to be a conserved quantity. Although only one independent fission channel f_c was adopted in the present study for a given (l,J) sequence of ^{241}Am, their number may generally be up to several. The numerous independent and mostly unknown capture channels $\gamma_c^{(k)}$ $(k = 1,\dots,N)$ are processed in the R-matrix theory by parametrizing the collision matrix in terms of the reduced R matrix of resonance parameters with the Reich-Moore approximation [2]. The reduced R matrix is given by the expression

$$R_{n\alpha_c}(E) = \sum_\lambda \frac{\chi_{\lambda n_c}\chi_{\lambda\alpha_c}}{E_{\lambda_c} - E - i\sum_k \chi^2_{\lambda\gamma_c^{(k)}}} + \mathcal{R}_c(E), \quad (3)$$

in which E_{λ_c} is a resonance energy in the (l,J) sequence, and $\chi_{\lambda\alpha_c}$ defines the reduced width amplitude of the resonance λ for either the elastic or the fission channel ($\alpha = n,f$). Since the independent single capture channels $\gamma_c^{(k)}$ are eliminated from α_c in terms of the Teichman-Wigner procedure [19], the reduced capture width amplitudes $\chi_{\lambda\gamma_c^{(k)}}$ appear in the denominator in a sum-square form. The amplitudes $\chi_{\lambda n_c}$, $\chi_{\lambda f_c}$, and $\chi_{\lambda\gamma_c^{(k)}}$ are related to the probability for the formation or decay of the compound state λ via the corresponding entrance or exit channel. These amplitudes are mostly transformed into partial widths $\Gamma_{\lambda n_c}$, $\Gamma_{\lambda f_c}$, and $\Gamma_{\lambda\gamma_c}$, where γ_c is the lumped (partial) capture channel of a given c. Thus, the relation between the neutron width and its corresponding amplitude is

$$\Gamma_{\lambda n_c} = 2P_l\chi^2_{\lambda n_c}, \quad (4)$$

where P_l denotes the centrifugal-barrier penetrability. In turn, the single channel fission width is constructed on a similar profile,

$$\Gamma_{\lambda f_c} = 2\chi^2_{\lambda f_c}, \quad (5)$$

whereas the total capture width is obtained as a sum of the single channel capture widths $\Gamma_{\lambda\gamma_c^{(k)}}$:

$$\Gamma_{\lambda\gamma_c} = \sum_k \Gamma_{\lambda\gamma_c^{(k)}} = 2\sum_k \chi^2_{\lambda\gamma_c^{(k)}}. \quad (6)$$

The background term $\mathcal{R}_c(E)$ of Eq. (3) was introduced by Wigner and Eisenbud [20] to account for the contribution of external levels found outside the range of the analysis. An explicit expression was proposed by Lynn in which $\mathcal{R}_c$ is complex [21]:

$$\mathcal{R}_c(E) = R_c^\infty + R_c^{\mathrm{loc}}(E) + i\pi s_c^{\mathrm{loc}}. \quad (7)$$

The real part of $\mathcal{R}_c$ can be split into contributions of neighboring (R_c^{loc}) and far-off levels (R_c^∞). Feshbach [22] assumes that only the immediate-neighbor resonances contribute appreciably to R_c^{loc}.

Throughout the R-matrix theory, R_c^∞ is called the distant level parameter. Its value is lower than unity [23]. Lynn indicates that the far-away contribution R_c^∞ modifies the channel radius a_c to give the effective hard-sphere potential scattering radius R'_c [24]. Denoting $R' = R'_c$ for the s-wave channel, one obtains

$$R' = a_0\left(1 - R_0^\infty\right). \quad (8)$$

The imaginary part $\mathrm{Im}[\mathcal{R}_c] = \pi s_c^{\mathrm{loc}}$ modifies the absorption cross section and adds a contribution that is inversely proportional to the velocity.

B. Unresolved resonance formalism

In the unresolved resonance range the average total cross section depends on the diagonal elements of the average collision matrix $\overline{U}_c$:

$$\overline{\sigma}_{tot_c}(E) = \frac{2\pi}{k^2} g_J (1 - \mathrm{Re}[\overline{U}_c(E)]), \tag{9}$$

The average partial reaction cross sections $\overline{\sigma}_{\alpha_c}$ for $\alpha = \gamma, f$ are calculated by means of the Hauser-Feshbach formula with width fluctuation corrections [25,26]:

$$\overline{\sigma}_{\alpha_c} = \frac{\pi}{k^2} g_J \frac{T_{n_c} T_{\alpha_c}}{\sum_\beta T_{\beta_c}} W_{n\alpha_c} \quad (\beta = n, n', \gamma, f), \tag{10}$$

where T_{α_c} and $W_{n\alpha_c}$ are the transmission coefficient and fluctuation correction factor, respectively, for capture or fission channel. Under classic narrow resonance approximation, the transmission coefficient is defined as

$$T_{\alpha_c}(E) = 2\pi \frac{\langle \Gamma_{\alpha_c} \rangle}{D_c}, \tag{11}$$

with D_c being the average level spacing and $\langle \Gamma_{\alpha_c} \rangle$ the corresponding average partial width. A rigorous independent definition and determination of the transmission coefficient is also possible and preferred. In that case a relation identical to Eq. (11) can be used to subsequently translate the rigorous T_{α_c} into an effective average partial width. Thus, for neutron channels the transmission coefficients T_{n_c} are usually determined from the average collision matrix elements:

$$T_{n_c} = 1 - |\overline{U}_c|^2. \tag{12}$$

The conversion from an (l,s,J) into an (l,J) channel formalism is performed for the average neutron widths in the unresolved resonance range by accounting the lumped neutron channels $c = (l,J)$ with degrees of freedom 1 or 2, which corresponds to the number of s-values contributing to the (l,J) sequence. Generally, the degree of freedom for an arbitrary channel α_c is determined by the number of the independent channels contributing to α_c. As a rule, equal average independent contributions are supposed, thus relating the width statistical behavior to the standard Porter-Thomas distribution.

In the frame of the R-matrix theory the analytical averaging of the collision matrix U in terms of average resonance parameters yields a diagonal collision matrix $\overline{U}$ with elements [27,28]

$$\overline{U}_c = e^{-2i\phi_c} \frac{\mathcal{B}_c + i P_l R_c^\infty - \frac{\pi S_c \sqrt{E} P_l}{2P_0}}{\mathcal{B}_c - i P_l R_c^\infty + \frac{\pi S_c \sqrt{E} P_l}{2P_0}}, \tag{13}$$

where ϕ_c is a hard-sphere phase shift for the channel radius a_c, S_c is the neutron strength function and the factor $\mathcal{B}_c$ depends on boundary condition parameters, which choice is often a matter of convenience in the R-matrix theory [29]. In the present work a "standard,, formulation is used, for which $\mathcal{B}_c = 1$ [17]. Under these conditions, Eq. (13) becomes

$$\overline{U}_c = e^{-2i\phi_c} \frac{1 + i P_l R_c^\infty - \frac{\pi S_c \sqrt{E} P_l}{2P_0}}{1 - i P_l R_c^\infty + \frac{\pi S_c \sqrt{E} P_l}{2P_0}}, \tag{14}$$

The analytically averaged collision matrix (14) can be equated to the optical model S matrix $\mathcal{S}_c$ expressed for further convenience through the diagonal C matrix:

$$\mathcal{S}_c = 1 + 2iC_c. \tag{15}$$

Thus, from Eqs. (14) and (15) one obtains the neutron strength function S_c and distant level parameter R_c^∞ derived from the link to the optical model:

$$P_l R_c^\infty = \frac{2\alpha_c \cos[2\phi_c] + (1 - 2\beta_c)\sin[2\phi_c]}{1 + 2\theta_c^2 - 2\beta_c + (1 - 2\beta_c)\cos[2\phi_c] - 2\alpha_c \sin[2\phi_c]}, \tag{16}$$

$$\frac{\pi S_c \sqrt{E} P_l}{2P_0} = \frac{2(\beta_c - \theta_c^2)}{1 + 2\theta_c^2 - 2\beta_c + (1 - 2\beta_c)\cos[2\phi_c] - 2\alpha_c \sin[2\phi_c]}. \tag{17}$$

The parameters α_c, β_c, and θ_c represent the real part, the imaginary part, and the absolute value of C_c:

$$\begin{aligned} \alpha_c &= \mathrm{Re}[C_c] \\ \beta_c &= \mathrm{Im}[C_c] \\ \theta_c &= |C_c| \end{aligned} \tag{18}$$

C. Channel radius for diffuse-edge potentials

The channel radius is one of the boundary conditions introduced in the R-matrix and optical model reaction formalisms to match the solution of the Schrodinger equation with its corresponding expression valid outside the region of nuclear forces. Such an abrupt separation of the configuration space by an imaginary closed surface of radius a_c lead to the notions of "internal" and "external" regions [30]. The complex mean-field potential $V(r)$ vanishes in the external region. If the real and imaginary parts of $V(r)$ are expressed as a sum of the volume (v), surface (s), and spin-orbit (so) components, the channel radius a_c satisfies the following condition (neutral incident particle):

$$\begin{aligned} &V(r) = V_v(r) + V_s(r) + V_{so}(r) \quad \text{for } r \leqslant a_c, \\ &V(r) \simeq 0 \quad \text{for } r > a_c. \end{aligned} \tag{19}$$

The size of the internal region is not defined. Therefore, the channel radii are more or less chosen arbitrarily. Mostly the channel radius a_c is defined as a simple function of the mass m of the target nucleus plus a constant term (ENDF convention) [31]:

$$a_c = 1.23\, m^{1/3} + 0.8 \text{ (infm)}. \tag{20}$$

Such a phenomenological representation dates back to 1950. Values of the parameters equal to 1.26 fm and 0.75 fm were reported by Drell in Ref. [32]. The order of magnitude of the constant term (0.8 fm) could also be explained by using the droplet model nuclear density distribution proposed by Myers [33] with a parametrization given in Ref. [34]. It takes into account the dilation due to several effects such as the surface tension, the neutron excess, and the Coulomb repulsion that occurs for finite nuclei.

The relationship between a_c and the nuclear radius R can be clarified assuming that the real part of the volume component of the nuclear mean-field has a diffuse edge of Woods-Saxon type with a midpoint radius equal to R and a diffuseness a:

$$f(r,R,a) = \frac{1}{1+e^{\frac{r-R}{a}}}. \quad (21)$$

Kapur and Peierls suggest making the internal region as small as possible but slightly larger than the radius R of the nucleus so that most of the mean field is in the internal region [30]. Similar prescriptions were given by Wigner and Eisenbud [20]. For simplicity, Vogt suggests choosing a channel radius greater than R by an amount roughly equal to the diffuseness [35]:

$$a_c \simeq R + a, \quad (22)$$

assuming that the A nucleons are uniformly distributed throughout a sphere of radius

$$R = r_0 A^{1/3}. \quad (23)$$

In optical model calculations, it is common to treat the reduced radius r_0 and the diffuseness a as adjustable parameters. These parameters can be determined by comparison with experimental data [36]. The value of r_0 is subject to variations from nuclide to nuclide with some evidence that r_0 is smaller for high values of A. Numerical calculations with global spherical optical models show that the reduced radius for the real part of the volume component lies in general between 1.23 and 1.3 fm. Among the optical model parameters reported in the Reference Input Parameter Library RIPL-3 [37], Morillon and Romain propose simple expressions for nuclei heavier than iron [38]:

$$r_0 = 1.295 - 2.7 \times 10^{-4}\ A \quad (\text{in fm}), \quad (24)$$

$$a = 0.566 + 5 \times 10^{-9}\ A^3 \quad (\text{in fm}). \quad (25)$$

Figure 1 shows that the combination of the empirical formula (22) with Eqs (24) and (25) provides values of a_c close to those calculated with the ENDF convention [Eq. (20)]. For the nuclear system ^{241}Am + n, we obtain respectively 8.28 and 8.46 fm. Figure 2 compares these results with the matter density distribution resulting from HFB calculations [39]. The lower plot indicates that Eq. (19) is not satisfied [$V(a_c) \neq 0$]. The empirical formulas (20) and (22) underestimate the magnitude of the expected channel radius by at least 1 fm.

D. Equivalent hard-sphere scattering radius

This inconsistency can be solved by using an equivalent hard-sphere radius deduced from the phase shift originating from the potential. As indicated by Eq. (19), the abrupt change of $V(r)$ at the channel radius introduces square-well phase shifts. Therefore, instead of using the empirical formulas (20) and (22), we can choose a_c such that the optical model and its equivalent square-well provide the same phase shifts at the common channel radii. Several works address this issue [23,40,41].

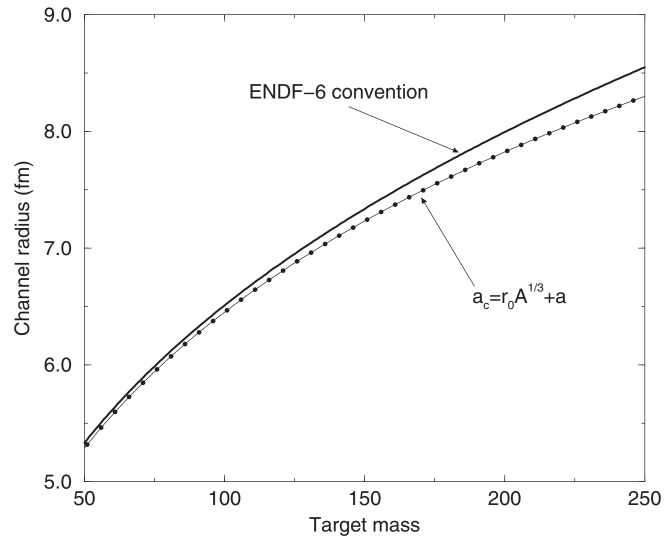

FIG. 1. Comparison of the channel radius calculated with the expressions (20) and (22). The reduced radius r_0 and the surface diffuseness a of the real part of the volume potential are calculated with Eqs (24) and (25).

The resonance theory [42] determines the hard-sphere phase shifts ϕ_l and centrifugal-barrier penetrabilities P_l from the precisely known radial wave functions at the channel radius a_c. Denoting $\rho = ka_c$, one obtains

$$\begin{aligned} \phi_0(\rho) &= \rho, \\ \phi_1(\rho) &= \rho - \tan^{-1}(\rho), \\ \phi_2(\rho) &= \rho - \tan^{-1}\left(\frac{3\rho}{3-\rho^2}\right), \end{aligned} \quad (26)$$

and

$$\begin{aligned} P_0(\rho) &= \rho, \\ P_1(\rho) &= \frac{\rho^3}{1+\rho^2}, \\ P_2(\rho) &= \frac{\rho^5}{9+3\rho^2+\rho^4}. \end{aligned} \quad (27)$$

Figure 3 shows the behavior of the J-dependent phase shifts for $l = 0,1,2$. Up to six spin configurations are possible with the ^{241}Am ground state spin $I = 5/2$. The coupled channel calculations were performed with the ECIS code [43] by using the dispersive optical model established in Ref. [44] with parameters reported in the Japanese Evaluated Nuclear Data Library JENDL-4. Equivalent hard-sphere radii for $c = \{l,J\}$ can be obtained from the least-squares fit of the optical model phase shifts with Eqs. (26). Results are reported in Table I.

In the resolved and unresolved resonance range, s-, p- and d-wave channel radii can be deduced from averaging the square of the J-dependent equivalent channel radius weighted by the statistical spin factor g_J:

$$a_l^2 = \frac{1}{2l+1} \sum_{s=|I-i|}^{I+i} \sum_{J=|l-s|}^{l+s} g_J a_{lJ}^2. \quad (28)$$

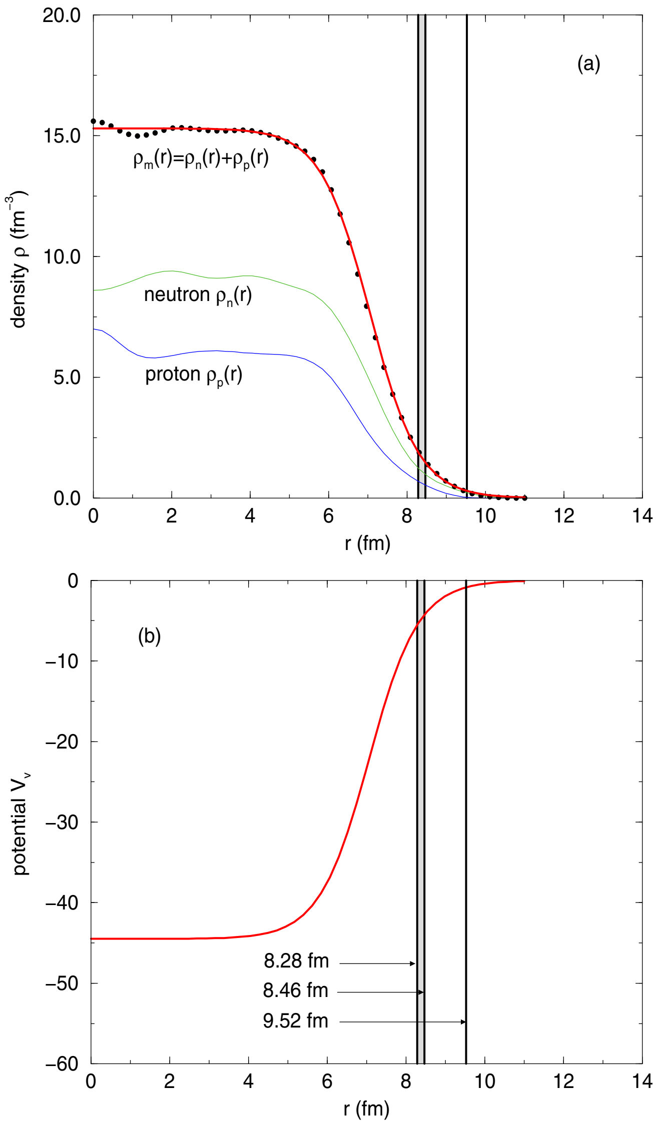

FIG. 2. (Color online) Matter density distribution (a) and real part of the volume potential (b) for the nuclear system ^{241}Am + n. The densities ρ_n and ρ_p are taken from the AMEDE database [39]. The channel radii a_c are taken from Table II.

Since the quantity to be averaged a_{lJ}^2 does not depend on s, Eq. (28) can also be presented as

$$a_l^2 = \frac{1}{2l+1}\sum_J \nu_{lJ} g_J a_{lJ}^2, \tag{29}$$

where the summation is over all possible J of a given l, and ν_{lJ} is the degree of freedom for the (l,J) sequence. For the nuclear system ^{241}Am + n, radii reported in Table I lead directly to

$$\begin{aligned} a_0 &= 9.52 \text{ fm},\\ a_1 &= 7.20 \text{ fm},\\ a_2 &= 8.76 \text{ fm}. \end{aligned} \tag{30}$$

The corresponding l-dependent phase shifts calculated with Eqs. (26) are compared in Fig. 4 with those deduced from the

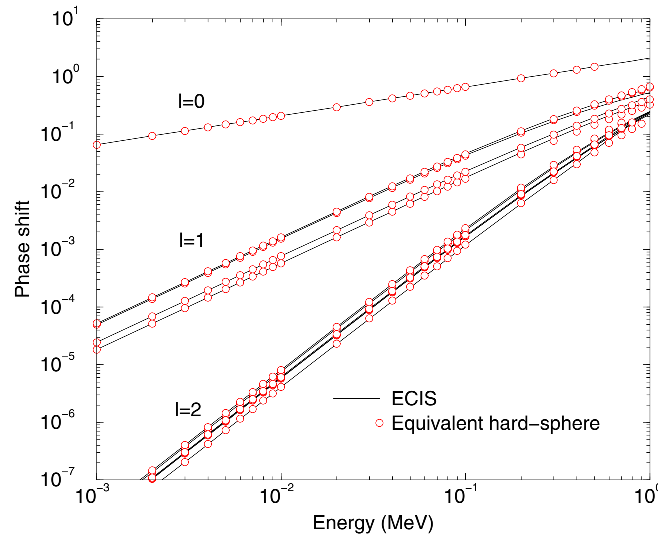

FIG. 3. (Color online) Energy dependence of the J-dependent phase shift for $l = 0,1,2$ calculated with the optical model code ECIS for the nuclear system ^{241}Am + n. The open circles represent the equivalent hard-sphere phase shift calculated with Eq. (26).

ECIS calculations. A good agreement is obtained between the hard-sphere approximation and the optical model calculations over a wide energy range. The larger discrepancies are observed for ϕ_1. They become higher than 5% above 300 keV.

Table II compares the a_0 value with those calculated with the phenomenological expressions (20) and (22). The hard-sphere approximation provides a higher s-wave radius which is in better agreement with the matter density distribution shown in Fig. 2. Its order of magnitude, closer to 10 fm, satisfies the condition $V(a_c) \simeq 0$ of Eq. (19).

These results show how the ideas of the optical model can be incorporated in the resonance theory in order that the elements of the R-matrix formalism no longer have an artificial dependence on the channel radii. The present channel radii were included in the ^{241}Am resonance analysis described in Sec. III. Impacts on the neutron strength functions are discussed in Sec. IV.

TABLE I. Equivalent hard-sphere channel radii obtained from the least-squares fit of the phase shift calculated by ECIS for the nuclear system ^{241}Am + n.

Total angular momentum	Statistical spin factor	Orbital momentum		
		$l = 0$	$l = 1$	$l = 2$
$J = 0$	1/12			9.26 fm
$J = 1$	3/12		5.51 fm	9.41 fm
$J = 2$	5/12	9.52 fm	7.66 fm	8.79 fm
$J = 3$	7/12	9.52 fm	7.81 fm	8.22 fm
$J = 4$	9/12		6.07 fm	8.83 fm
$J = 5$	11/12			8.88 fm

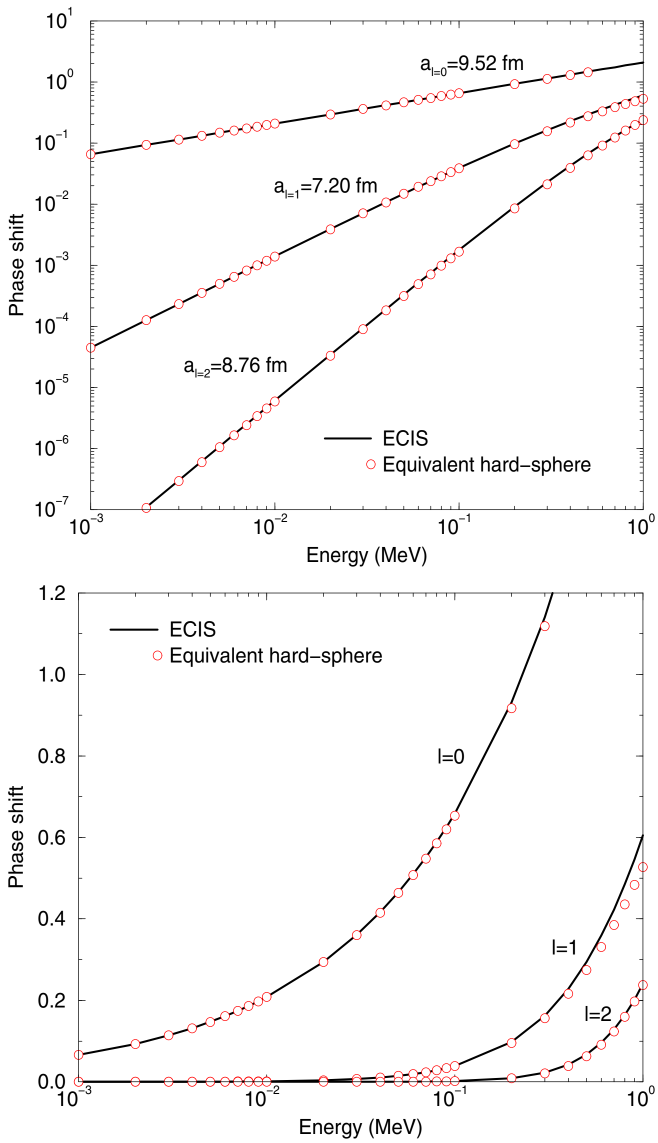

FIG. 4. (Color online) Comparison of the l-dependent phase shift calculated with the hard-sphere approximation ($a_0 = 9.52$ fm, $a_1 = 7.20$ fm, and $a_2 = 8.76$ fm) and calculated with the optical model code ECIS for the nuclear system ^{241}Am + n in log-log and log-lin scales.

III. NEUTRON SPECTROSCOPY OF ^{241}Am

A. Experimental data

Resonance parameters for ^{241}Am + n were derived by adjusting them in a least-squares fit to experimental data that are reported in the EXFOR library together with the data reported by Lampoudis *et al.* [5]. From a simultaneous analysis of the data sets listed in Table III, energies and partial widths of 211 resonances ($l = 0$) up to 150 eV were determined.

In the analysis, the transmission data of Lampoudis *et al.* [5] were considered as a reference. They were obtained from measurements at a 26.45 m station of GELINA with a homogeneous sample prepared by the sol-gel method. The sample, with an areal density of $n = (2.068 \pm 0.010) \times 10^{-4}$ at/b, was especially designed to derive accurate parameters for the strong s-wave resonances at 0.306, 0.574, and 1.270 eV. The AGS concept [45] was used to derive the transmission and propagate both correlated and uncorrelated uncertainties. In addition, the experimental conditions, including the sample characteristics and covariance data, are fully documented following the recommendations of Ref. [46]. The transmission data of Derrien and Lucas [47] were obtained from measurements at 17.9 and 53.4 m stations using three AmO_2 samples with different areal density, i.e., 0.18, 0.63, and 1.87 g/cm^2. The results of the three data sets were merged into one single experimental total cross section from 0.8 eV to 1 keV so that the individual transmissions are not reported in EXFOR. As noted in Ref. [48], parameters of strong resonances derived from measurements with powder samples will be biased, unless their particle size distributions are taken into account in the analysis. Unfortunately not enough details are provided to account for the particle size distribution by the procedure that has been implemented in REFIT [49,50]. To reduce bias effects due to the sample properties an average areal density was determined from a fit to the data and the transmission data involving the strong resonances with energies below 8 eV were not included in the fit.

Since the neutron widths for most of the low energy resonances are much smaller than their radiation widths, the neutron widths derived from the transmission data of Lampoudis *et al.* were used to normalize the capture yields of Refs. [5,6,51]. The capture data of Lampoudis *et al.* [5] were obtained from experiments with a detection system consisting of two C_6D_6 detectors using the same sample as the one used for the transmission measurements. The energy dependence of the neutron flux was derived in parallel from measurements with a detector placed one meter before the sample. The detector consisted of two ionization chambers with a common cathode loaded with two layers of ^{10}B. Fixed background filters were used to reduce bias effects due to the background corrections [48] and the results of the transmission data were used to normalize the capture data. Given the low amount of ^{241}Am in the sample the impact of the neutron flux attenuation in the sample was negligible and no correction due to the attenuation of the neutron beam was required.

Van Praet *et al.* [51] derived a capture yield from measurements with C_6D_6 detectors at a 8.6 m station of GELINA. The neutron flux was measured with a B_4C disk at the place of the capture sample. Although a relatively thick metallic ^{241}Am sample (areal density of 1.063×10^{-3} at/b) was used, no special procedure was applied to correct for the neutron attenuation and related gamma-ray transport in the sample. The capture yield of Jandel *et al.* [6] resulted from measurements at LANSCE with a 4π total absorption

TABLE II. Comparison of the equivalent hard-sphere channel radii obtained for the nuclear system ^{241}Am + n and calculated with Eqs. (20) and (22).

Channel radius		Ref.	Value
ENDF convention	Eq. (20)	[31]	8.46 fm
Vogt's prescription	Eq. (22)	[35]	8.28 fm
Equivalent hard-sphere ($l = 0$)			9.52 fm

TABLE III. Experimental characteristics of the capture, fission, and transmission data used in this work.

Author Reference	Jandel [6]	Van Praet [51]	Van Praet [51]	Lampoudis [5]	Lampoudis [5]	Derrien [47]	Derrien [47]	Derrien [47]	Dabbs [52]
Year	2008	1985	1985	2013	2013	1975	1975	1975	1983
Facility	DANCE	GELINA	GELINA	GELINA	GELINA	Saclay LINAC	Saclay LINAC	Saclay LINAC	ORELA
Data type	Capture yield	Capture yield	Capture yield	Capture yield	Transmission	Transmission	Transmission	Fission	Fission
Energy range (eV)	$E<3.0$	1.6–13.5	13.5–160	$E<73.0$	$E<40.0$	8.8–27.0	27.0–160.0	1.0–40.0	$E<160.0$
Flight length (m)	22.2	8.6	8.6	12.9	26.4	17.9	53.4		9.1
Sample diam. (mm)	6.35	20.0×20.0	20.0×20.0	22.34	22.34				76.2
Sample thick. (mm)		0.32	0.32	2.17	2.17				
Areal density (at/b)	1.080×10^{-7}	1.063×10^{-3}	1.063×10^{-3}	2.068×10^{-4} $\pm0.010\times10^{-4}$	2.068×10^{-4} $\pm0.010\times10^{-4}$	1.273×10^{-3}[a] $\pm0.063\times10^{-3}$	4.083×10^{-3}[a] $\pm0.160\times10^{-3}$		
Normalization	1.166 ±0.034	1.077 ±0.030	1.022 ±0.030	0.987 ±0.020				1.00 ±0.06	1.00 ±0.04

[a] ^{241}Am area density determined from the least-squares fit of the transmission data.

detector placed at 20.2 m from the neutron producing target. A thin ^{241}Am sample, prepared by electroplating was used. The normalization was based on the nonsaturated yield of the 4.9 eV resonance resulting from additional measurements with a Au sample which was characterized by Rutherford backscattering spectrometry.

All experiments reported in Table III were carried out at a moderated pulsed neutron beam. The response functions at a moderated beam are dominated by the neutron transport in the target-moderator assembly [53]. They can be approximated by a chi-square distribution and expressed in terms of an equivalent distance. The width of the corresponding distribution is proportional to the neutron mean free path which strongly depends on the size of the target/moderator assembly.

The REFIT code was used to perform a simultaneous analysis of the data reported in Table III. The latest version of the code accounts for various experimental effects like Doppler broadening, neutron self-shielding, multiple interaction, sample inhomogeneities, neutron sensitivity of the detection system, gamma-ray attenuation in the sample, and the response of the TOF spectrometer [48]. Only uncorrelated uncertainties are propagated. To account for the uncertainties of systematic effects the Monte Carlo procedure proposed by De Saint Jean [54] was applied. This procedure was used to propagate the uncertainties on the equivalent distance ($\Delta L = 1$ cm), time offset ($\Delta t_0 = 1$ ns), sample temperature ($\Delta T = 5$ K), the normalizaton factors, and areal densities. The normalization and areal density uncertainties are specified in Table III. This procedure is equivalent to a Bayesian analysis by renormalizing the posterior multidimensional probability density function such that the marginal probability distributions of the experimental parameters are identical to their prior distribution [55].

B. Results and discussions

The initial parameters of the unbound (positive) resonances, including their spin and parity, were taken from the JEFF-3.1.1 data library. No attempt was made to change the spin of the resonances and they were all supposed to be s-wave resonances ($l = 0$). The effective scattering radius was set to $R' = 9.52$ fm. The distant level parameter R_c^∞ was set to zero, such that the channel radius equals the effective scattering radius, i.e., $a_c = R'$.

Since the observed resonances only contribute for 30% to the capture cross section at thermal energy [5], there is a substantial contribution from negative resonances (bound states). Figure 5 compares the experimental capture yield of Lampoudis *et al.* [5] with the yield resulting from a fit with a single negative resonance and one with an external contribution due to the term $s_c^{\rm loc}$ in Eq. (7). The latter produces a contribution with a pure $1/v$ energy dependence. The results in Fig. 5 suggest that the external contribution in the capture cross section of ^{241}Am originates from a bound state with a $1/v$ energy dependence, as already noticed in Ref. [56]. In the final analysis two bound states, related respectively to each possible s-wave resonance spin, were included to describe the capture yield in the thermal energy region. The resulting parameters are listed in Table IV and compared with the neutron and radiation widths reported in Ref. [5]. Results of the least-squares fit are shown in Figs. 6, 7 and 8. A comparison of the neutron widths with those reported by Lampoudis *et al.* [5] and Jandel *et al.* [6] and with the ones adopted in the JEFF-3.1.1 library is shown in Fig. 9.

Evidently, the resulting capture cross section at thermal energy and the parameters for low energy resonances are fully consistent with the thermal capture cross section (749 ± 35) barns and parameters reported by Lampoudis *et al.* [5]. At energies above about 30 eV the impact of other data sets becomes more important. To derive consistent parameters from the data of Derrien and Lucas [47], the average areal density for these data had to be reduced. Such a reduction is expected to account for inhomogeneities due to the grain size distribution of the powder samples as discussed in Ref. [57]. Figure 9 shows that the neutron widths obtained in this work are about 20% larger compared to those recommended in the JEFF-3.1.1 evaluated data library, which is largely based on the results reported by Derrien and Lucas [47]. Hence, this difference can

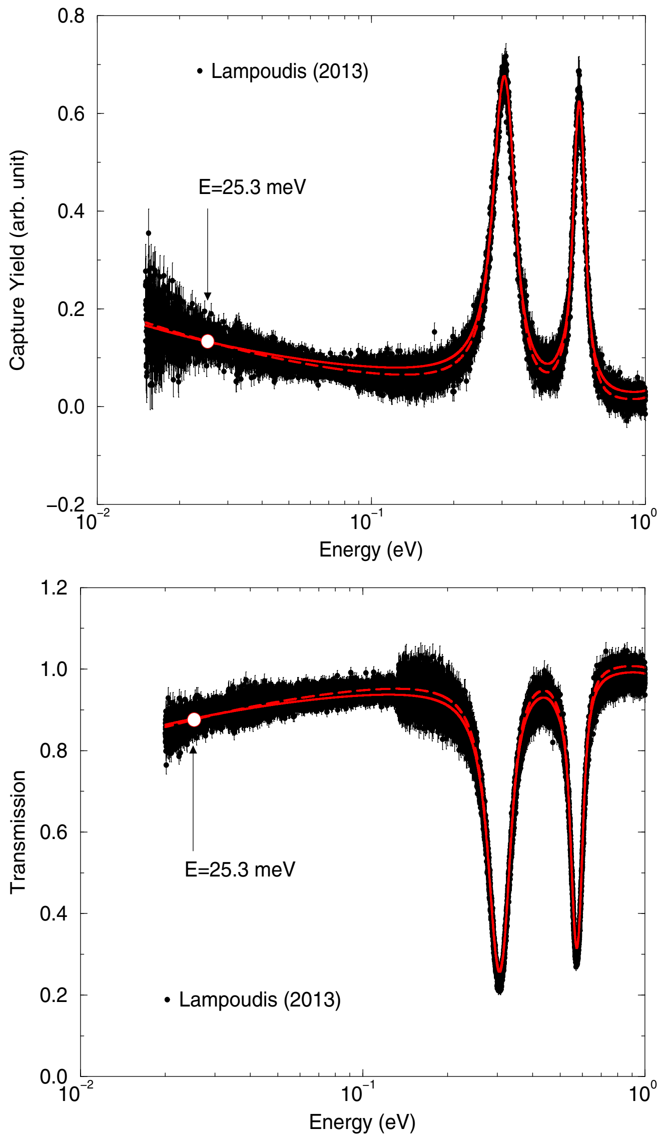

FIG. 5. (Color online) Low neutron energy part of the capture yield and transmission data measured at the IRMM. The theoretical curves were calculated with the REFIT code. The solid line was obtained by using $\mathrm{Im}[\mathcal{R}_c] = (7.6 \pm 0.5) \times 10^{-3}$ and $\mathrm{Re}[\mathcal{R}_c] = 0$. The dashed line was obtained with the resonance parameters reported in Ref. [5]. The open circles indicate the thermal values.

be explained by the above mentioned bias due to the sample properties.

Including the data of Van Praet *et al.* [51] in the analysis is not straightforward. The results in Fig. 6 illustrate that they suffer from a bias effect which increases with increasing resonance strength. Such an effect can be due to the use of a relatively thick sample. Capture data resulting from measurements with thick samples require special corrections to account for the gamma-ray transport in the sample as discussed in Refs. [48,58]. According to the description in Ref. [51] such corrections have not been applied. Unfortunately not enough information is available to apply the correction. Therefore, in the analysis the strong low energy resonances ($E < 8$ eV) were excluded. A good agreement with the rest of their data was obtained by applying a normalization factor 1.077 ± 0.028 for energies below 13.5 eV and 1.022 ± 0.025 for energies above.

To obtain a good quality of the fit to the capture data of Jandel *et al.* [6] their yield was increased by more than 15% over the whole energy region. This correction can result from a bias due to their normalization method as suggested in Ref. [5]. The systematic underestimation of their yield leads to their thermal capture cross section of 665 ± 33 barns which is about 10% lower than 749 ± 35 barns. Also the neutron widths reported by Fraval *et al.* [59] as derived from capture measurements at the nTOF facility at CERN are systematically lower. The difference becomes smaller with increasing energy. For energies below 30 eV their neutron width are on average 10% lower compared to those in Table IV. Also their capture cross section at thermal energy is lower by about 10%.

IV. AVERAGE RESONANCE PARAMETERS

The average resonance parameters of interest for a partial-wave breakdown of the neutron cross sections in the resonance region are the mean level spacing, the neutron strength function, and the average radiation and fission widths. Parameters for s-wave levels are determined from a statistical analysis of the resolved resonance parameters listed in Table IV. For higher values of angular momentum $l > 0$, average resonance parameters are obtained from systematics and by means of optical and statistical model codes.

A. Average radiation width

For 14 resonances both the neutron and radiation width were determined. Figure 10 shows the resulting $\Gamma_{\lambda\gamma_c}$ as a function of energy together with the values reported in the literature. Large spreading ranging from 39.5 to 47.3 meV is observed. From these data an average radiation width of $\langle \Gamma_{\gamma_0} \rangle = 43.3 \pm 1.1$ meV was derived. This average value is in good agreement with the average value reported by Derrien and Lucas [47] and Lampoudis *et al.* [5]. In cases where the the radiation width could not be determined, the average value was adopted.

B. Statistical analysis with the ESTIMA method

Detailed explanations on the ESTIMA method [12] were given in previous works [9–11]. The method determines simultaneously the most probable neutron strength function and mean level spacing for s-wave levels from the properties of the cumulative Porter-Thomas distribution of reduced neutron widths [61]. The latter assumes that the reduced neutron widths in the channel $c = \{l, J\}$,

$$\Gamma^{l}_{n_J} = \Gamma_{\lambda n_c} \frac{P_0}{P_l} \sqrt{\frac{1\mathrm{eV}}{E_{\lambda_c}}} \qquad (31)$$

have a chi-squared distribution with one degree of freedom (i.e., a Porter-Thomas distribution). In the analysis no distinction between resonances with different J was made. Calculations were performed on the s-wave neutron widths weighted by the statistical spin factor g_J. The cumulative

TABLE IV. ^{241}Am s-wave resonance parameters below 150 eV. The spins of the resonances are assumed from the JEFF-3.1.1 evaluation. The capture width equal to 43.3 ± 1.1 meV, which is an average width determined in present study, is also assumed in the analysis.

		This work			Lampoudis *et al.* [5]	
E_{λ_c} (eV)	J^π ($\hbar$)	$\Gamma_{\lambda\gamma_c}$ (meV)	$\Gamma_{\lambda n_c}$ (meV)	$\Gamma_{\lambda f_c}$ (meV)	$\Gamma_{\lambda\gamma_c}$ (meV)	$\Gamma_{\lambda n_c}$ (meV)
−0.421	3^-	43.3	0.173	0.063		
−0.378	2^-	43.3	0.528	0.225		
−0.363	2^-				42.0	0.660
0.306 ± 0.001	3^-	40.7 ± 0.3	0.063 ± 0.002	0.212 ± 0.009	41.6 ± 0.4	0.064 ± 0.001
0.574 ± 0.001	2^-	39.6 ± 0.7	0.148 ± 0.005	0.080 ± 0.003	42.1 ± 0.6	0.151 ± 0.001
1.270 ± 0.002	3^-	41.3 ± 0.8	0.375 ± 0.012	0.269 ± 0.008	41.7 ± 0.8	0.373 ± 0.004
1.919 ± 0.003	3^-	40.6 ± 0.8	0.124 ± 0.005	0.046 ± 0.003	43.9 ± 1.1	0.126 ± 0.001
2.362 ± 0.004	2^-	42.1 ± 0.8	0.110 ± 0.004	0.138 ± 0.007	48.6 ± 2.1	0.121 ± 0.002
2.586 ± 0.004	3^-	43.3 ± 0.6	0.163 ± 0.006	0.122 ± 0.006	42.2 ± 1.6	0.164 ± 0.002
3.964 ± 0.004	2^-	43.2 ± 0.8	0.314 ± 0.011	0.119 ± 0.006	42.1 ± 2.0	0.307 ± 0.004
4.957 ± 0.006	3^-	42.9 ± 1.7	0.185 ± 0.006	0.319 ± 0.015	43.2 ± 3.3	0.184 ± 0.005
5.404 ± 0.007	2^-	43.7 ± 1.9	1.140 ± 0.030	0.488 ± 0.021	43.4 ± 1.3	1.123 ± 0.011
6.102 ± 0.009	3^-	43.3 ± 1.1	0.131 ± 0.004	0.282 ± 0.014	50.0 ± 7.0	0.140 ± 0.006
6.725 ± 0.010	3^-	43.3 ± 1.1	0.030 ± 0.001	0.111 ± 0.007		
7.642 ± 0.012	2^-	43.3 ± 1.1	0.057 ± 0.002	0.062 ± 0.004		
8.149 ± 0.012	3^-	43.3 ± 1.1	0.115 ± 0.004	0.102 ± 0.005	42.0	0.112 ± 0.006
9.099 ± 0.010	2^-	46.2 ± 2.7	0.571 ± 0.020	0.165 ± 0.008	33.7 ± 4.0	0.539 ± 0.017
9.834 ± 0.011	3^-	47.2 ± 3.0	0.426 ± 0.015	0.862 ± 0.034	51.5 ± 5.6	0.452 ± 0.013
10.101 ± 0.015	2^-	43.3 ± 1.1	0.038 ± 0.002	0.149 ± 0.016		
10.385 ± 0.012	3^-	46.4 ± 3.3	0.345 ± 0.012	0.057 ± 0.003	42.0	0.347 ± 0.009
10.978 ± 0.013	2^-	47.0 ± 3.4	0.594 ± 0.021	0.099 ± 0.005	42.0	0.570 ± 0.195
11.577 ± 0.027	3^-	43.3 ± 1.1	0.019 ± 0.002	0.214 ± 0.018		
12.124 ± 0.028	3^-	43.3 ± 1.1	0.009 ± 0.002	0.080 ± 0.008		
12.859 ± 0.032	2^-	43.3 ± 1.1	0.195 ± 0.008	0.049 ± 0.004	42.0	0.199 ± 0.015
13.848 ± 0.021	3^-	43.3 ± 1.1	0.014 ± 0.003	0.059 ± 0.005		
14.337 ± 0.022	2^-	43.3 ± 1.1	0.099 ± 0.019	0.067 ± 0.005		
14.657 ± 0.019	3^-	42.2 ± 2.7	2.459 ± 0.100	0.222 ± 0.014	42.0	2.575 ± 0.033
15.668 ± 0.024	2^-	43.3 ± 1.1	0.354 ± 0.013	0.104 ± 0.008	42.0	0.346 ± 0.021
16.363 ± 0.023	3^-	43.3 ± 1.1	1.300 ± 0.056	0.093 ± 0.007	42.0	1.358 ± 0.031
16.824 ± 0.024	2^-	43.3 ± 1.1	0.932 ± 0.034	0.256 ± 0.018	42.0	0.971 ± 0.030
17.701 ± 0.027	3^-	43.3 ± 1.1	0.408 ± 0.015	0.256 ± 0.018	42.0	0.385 ± 0.020
18.137 ± 0.027	2^-	43.3 ± 1.1	0.031 ± 0.006	0.115 ± 0.010		
19.410 ± 0.049	3^-	43.3 ± 1.1	0.220 ± 0.011	0.264 ± 0.014	42.0	0.250 ± 0.020
20.293 ± 0.047	3^-	43.3 ± 1.1	0.033 ± 0.006	0.193 ± 0.014		
20.843 ± 0.053	2^-	43.3 ± 1.1	0.123 ± 0.010	0.226 ± 0.013		
21.717 ± 0.056	3^-	43.3 ± 1.1	0.093 ± 0.006	0.208 ± 0.013		
22.709 ± 0.053	3^-	43.3 ± 1.1	0.082 ± 0.010	0.155 ± 0.011		
23.035 ± 0.059	2^-	43.3 ± 1.1	0.609 ± 0.025	0.252 ± 0.012	42.0	0.568 ± 0.050
23.289 ± 0.061	3^-	43.3 ± 1.1	0.462 ± 0.021	0.125 ± 0.007	42.0	0.516 ± 0.038
24.144 ± 0.025	3^-	43.3 ± 1.1	1.321 ± 0.052	0.140 ± 0.007	42.0	1.320 ± 0.038
25.584 ± 0.028	3^-	43.3 ± 1.1	1.289 ± 0.051	0.321 ± 0.016	42.0	1.345 ± 0.050
26.446 ± 0.030	2^-	43.3 ± 1.1	0.756 ± 0.068	0.064 ± 0.005	42.0	0.739 ± 0.069
26.626 ± 0.040	3^-	43.3 ± 1.1	0.204 ± 0.043	0.175 ± 0.010		
27.557 ± 0.043	2^-	43.3 ± 1.1	0.357 ± 0.043	0.613 ± 0.042	42.0	0.914 ± 0.052
27.694 ± 0.043	3^-	43.3 ± 1.1	0.377 ± 0.019	0.159 ± 0.008	42.0	0.031 ± 0.060
28.302 ± 0.044	2^-	43.3 ± 1.1	0.803 ± 0.024	0.113 ± 0.007	42.0	0.874 ± 0.065
28.846 ± 0.045	3^-	43.3 ± 1.1	0.457 ± 0.014	0.168 ± 0.010	42.0	0.422 ± 0.040
29.448 ± 0.046	3^-	43.3 ± 1.1	0.690 ± 0.020	0.102 ± 0.006	42.0	0.718 ± 0.053
29.869 ± 0.046	2^-	43.3 ± 1.1	0.090 ± 0.005	0.304 ± 0.022		
30.784 ± 0.048	3^-	43.3 ± 1.1	0.198 ± 0.015	0.360 ± 0.024	42.0	0.289 ± 0.086
30.985 ± 0.048	2^-	43.3 ± 1.1	0.487 ± 0.027	0.305 ± 0.019	42.0	0.594 ± 0.344
31.190 ± 0.049	3^-	43.3 ± 1.1	0.952 ± 0.028	0.207 ± 0.011	42.0	0.898 ± 0.302
31.967 ± 0.051	2^-	43.3 ± 1.1	0.431 ± 0.015	0.250 ± 0.015		
33.511 ± 0.052	3^-	43.3 ± 1.1	0.064 ± 0.006	0.101 ± 0.008		

TABLE IV. (*Continued.*)

		This work			Lampoudis *et al.* [5]	
E_{λ_c} (eV)	J^π ($\hbar$)	$\Gamma_{\lambda\gamma_c}$ (meV)	$\Gamma_{\lambda n_c}$ (meV)	$\Gamma_{\lambda f_c}$ (meV)	$\Gamma_{\lambda\gamma_c}$ (meV)	$\Gamma_{\lambda n_c}$ (meV)
33.970 ± 0.051	2^-	43.3 ± 1.1	0.864 ± 0.031	0.021 ± 0.002	42.0	1.231 ± 0.090
34.404 ± 0.053	3^-	43.3 ± 1.1	0.135 ± 0.009	0.561 ± 0.036		
34.869 ± 0.053	2^-	43.3 ± 1.1	0.854 ± 0.030	0.161 ± 0.010	42.0	0.992 ± 0.086
35.423 ± 0.053	3^-	43.3 ± 1.1	0.410 ± 0.016	0.144 ± 0.010	42.0	0.490 ± 0.056
36.228 ± 0.055	3^-	43.3 ± 1.1	0.189 ± 0.019	0.142 ± 0.011		
36.513 ± 0.055	2^-	43.3 ± 1.1	0.168 ± 0.016	0.168 ± 0.011		
36.919 ± 0.048	3^-	43.3 ± 1.1	3.162 ± 0.099	0.429 ± 0.022	42.0	3.631 ± 0.102
37.844 ± 0.057	3^-	43.3 ± 1.1	0.044 ± 0.009	0.417 ± 0.034		
38.305 ± 0.050	2^-	43.3 ± 1.1	3.039 ± 0.095	0.305 ± 0.016	42.0	3.414 ± 0.128
38.681 ± 0.058	3^-	43.3 ± 1.1	0.056 ± 0.012	0.365 ± 0.024		
39.550 ± 0.060	3^-	43.3 ± 1.1	1.269 ± 0.046	0.315 ± 0.017	42.0	1.496 ± 0.051
39.834 ± 0.062	2^-	43.3 ± 1.1	0.137 ± 0.042	0.604 ± 0.041		
40.036 ± 0.062	2^-	43.3 ± 1.1	0.694 ± 0.045	0.606 ± 0.036	42.0	0.949 ± 0.129
40.344 ± 0.062	3^-	43.3 ± 1.1	0.855 ± 0.037	0.079 ± 0.005	42.0	0.938 ± 0.083
41.267 ± 0.064	2^-	43.3 ± 1.1	0.136 ± 0.014	0.471 ± 0.032		
41.726 ± 0.063	3^-	43.3 ± 1.1	0.365 ± 0.016	0.111 ± 0.008		
42.072 ± 0.065	2^-	43.3 ± 1.1	0.235 ± 0.013	0.217 ± 0.015		
43.227 ± 0.067	3^-	43.3 ± 1.1	0.903 ± 0.033	0.093 ± 0.006	42.0	0.946 ± 0.234
43.524 ± 0.067	2^-	43.3 ± 1.1	0.791 ± 0.035	0.222 ± 0.014	42.0	1.346 ± 0.403
44.356 ± 0.069	3^-	43.3 ± 1.1	0.167 ± 0.010	0.200 ± 0.014		
44.873 ± 0.069	3^-	43.3 ± 1.1	0.122 ± 0.008	0.148 ± 0.011		
45.998 ± 0.107	2^-	43.3 ± 1.1	0.933 ± 0.067	0.083 ± 0.006	42.0	0.876 ± 0.109
46.495 ± 0.108	3^-	43.3 ± 1.1	0.392 ± 0.062	0.108 ± 0.008	42.0	0.479 ± 0.095
47.442 ± 0.121	2^-	43.3 ± 1.1	1.331 ± 0.161	0.305 ± 0.019	42.0	1.400 ± 0.130
47.734 ± 0.111	2^-	43.3 ± 1.1	0.087 ± 0.024	0.626 ± 0.047		
48.701 ± 0.042	3^-	43.3 ± 1.1	0.707 ± 0.031	0.141 ± 0.017	42.0	0.756 ± 0.100
49.262 ± 0.044	3^-	43.3 ± 1.1	0.221 ± 0.014	0.371 ± 0.053		
49.841 ± 0.077	2^-	43.3 ± 1.1	0.091 ± 0.023	0.369 ± 0.122		
50.218 ± 0.044	2^-	43.3 ± 1.1	3.267 ± 0.130	0.304 ± 0.019	42.0	3.050 ± 0.111
50.790 ± 0.043	3^-	43.3 ± 1.1	0.420 ± 0.022	0.213 ± 0.034	42.0	0.546 ± 0.126
51.920 ± 0.058	2^-	43.3 ± 1.1	1.950 ± 0.083	0.212 ± 0.015	42.0	2.010 ± 0.173
52.296 ± 0.039	3^-	43.3 ± 1.1	0.048 ± 0.017	0.597 ± 0.133		
52.933 ± 0.039	3^-	43.3 ± 1.1	0.216 ± 0.019	0.080 ± 0.036		
53.399 ± 0.040	2^-	43.3 ± 1.1	0.299 ± 0.027	0.155 ± 0.042		
54.308 ± 0.040	3^-	43.3 ± 1.1	0.139 ± 0.019	0.099 ± 0.030		
54.765 ± 0.041	3^-	43.3 ± 1.1	0.355 ± 0.111	0.200 ± 0.019		
54.960 ± 0.065	2^-	43.3 ± 1.1	1.431 ± 0.146	0.291 ± 0.021	42.0	1.745 ± 0.159
55.503 ± 0.041	3^-	43.3 ± 1.1	0.243 ± 0.025	0.264 ± 0.041		
55.869 ± 0.059	2^-	43.3 ± 1.1	1.988 ± 0.199	0.040 ± 0.003	42.0	1.409 ± 0.351
56.076 ± 0.042	3^-	43.3 ± 1.1	0.922 ± 0.070	0.213 ± 0.017	42.0	1.391 ± 0.248
56.601 ± 0.042	2^-	43.3 ± 1.1	0.098 ± 0.027	0.120 ± 0.035		
57.230 ± 0.087	3^-	43.3 ± 1.1	3.298 ± 0.179	0.119 ± 0.009	42.0	4.028 ± 0.175
57.413 ± 0.089	2^-	43.3 ± 1.1	0.695 ± 0.221	1.187 ± 0.087		
58.100 ± 0.090	3^-	43.3 ± 1.1	0.057 ± 0.011	0.351 ± 0.110		
58.943 ± 0.083	2^-	43.3 ± 1.1	0.678 ± 0.032	0.305 ± 0.034	42.0	0.707 ± 0.150
59.913 ± 0.090	3^-	43.3 ± 1.1	0.260 ± 0.017	0.090 ± 0.033		
60.262 ± 0.093	2^-	43.3 ± 1.1	0.154 ± 0.015	0.080 ± 0.031		
61.129 ± 0.091	3^-	43.3 ± 1.1	1.571 ± 0.078	0.239 ± 0.019	42.0	1.909 ± 0.140
61.471 ± 0.095	2^-	43.3 ± 1.1	0.666 ± 0.055	0.626 ± 0.047		
61.787 ± 0.096	3^-	43.3 ± 1.1	0.022 ± 0.004	0.250 ± 0.099		
62.426 ± 0.086	3^-	43.3 ± 1.1	0.210 ± 0.018	0.265 ± 0.061		
63.391 ± 0.098	3^-	43.3 ± 1.1	0.135 ± 0.012	0.091 ± 0.041		
63.945 ± 0.099	2^-	43.3 ± 1.1	5.732 ± 0.276	0.293 ± 0.021	42.0	5.814 ± 0.271
64.446 ± 0.100	3^-	43.3 ± 1.1	1.984 ± 0.107	0.201 ± 0.016	42.0	2.349 ± 0.206
65.073 ± 0.101	2^-	43.3 ± 1.1	7.113 ± 0.327	0.492 ± 0.035	42.0	7.842 ± 0.406

TABLE IV. (*Continued.*)

		This work			Lampoudis *et al.* [5]	
E_{λ_c} (eV)	J^π ($\hbar$)	$\Gamma_{\lambda\gamma_c}$ (meV)	$\Gamma_{\lambda n_c}$ (meV)	$\Gamma_{\lambda f_c}$ (meV)	$\Gamma_{\lambda\gamma_c}$ (meV)	$\Gamma_{\lambda n_c}$ (meV)
65.638 ± 0.104	3^-	43.3 ± 1.1	1.165 ± 0.058	0.398 ± 0.033	42.0	0.985 ± 0.157
66.217 ± 0.103	2^-	43.3 ± 1.1	1.376 ± 0.072	0.297 ± 0.026		
66.785 ± 0.104	3^-	43.3 ± 1.1	1.827 ± 0.092	0.168 ± 0.015	42.0	2.026 ± 0.179
68.411 ± 0.104	2^-	43.3 ± 1.1	0.672 ± 0.039	0.609 ± 0.059		
69.487 ± 0.108	3^-	43.3 ± 1.1	1.246 ± 0.079	0.070 ± 0.010	42.0	0.428 ± 0.038
69.726 ± 0.108	2^-	43.3 ± 1.1	3.646 ± 0.205	0.180 ± 0.015	42.0	5.638 ± 2.495
71.132 ± 0.110	3^-	43.3 ± 1.1	0.631 ± 0.097	0.124 ± 0.027		
71.358 ± 0.112	2^-	43.3 ± 1.1	1.637 ± 0.121	0.306 ± 0.025	42.0	2.115 ± 0.345
71.744 ± 0.111	3^-	43.3 ± 1.1	1.071 ± 0.066	0.254 ± 0.023	42.0	1.409 ± 0.386
72.223 ± 0.112	3^-	43.3 ± 1.1	0.286 ± 0.043	0.206 ± 0.053		
74.436 ± 0.173	2^-	43.3 ± 1.1	0.208 ± 0.019	0.120 ± 0.042		
74.872 ± 0.167	2^-	43.3 ± 1.1	0.735 ± 0.046	0.221 ± 0.029		
75.564 ± 0.175	3^-	43.3 ± 1.1	0.410 ± 0.042	0.080 ± 0.029		
75.821 ± 0.167	2^-	43.3 ± 1.1	0.833 ± 0.066	0.185 ± 0.021		
76.479 ± 0.178	3^-	43.3 ± 1.1	0.119 ± 0.012	0.299 ± 0.084		
76.853 ± 0.178	3^-	43.3 ± 1.1	0.109 ± 0.012	0.579 ± 0.085		
78.072 ± 0.172	2^-	43.3 ± 1.1	2.315 ± 0.121	0.125 ± 0.014	42.0	2.513 ± 0.534
78.444 ± 0.174	3^-	43.3 ± 1.1	1.089 ± 0.060	0.197 ± 0.021	42.0	1.208 ± 0.334
79.424 ± 0.180	3^-	43.3 ± 1.1	0.761 ± 0.046	0.250 ± 0.032		
79.922 ± 0.186	2^-	43.3 ± 1.1	0.845 ± 0.083	0.264 ± 0.025		
80.274 ± 0.182	3^-	43.3 ± 1.1	0.634 ± 0.049	0.408 ± 0.112		
81.018 ± 0.188	2^-	43.3 ± 1.1	0.336 ± 0.032	0.191 ± 0.058		
81.347 ± 0.183	3^-	43.3 ± 1.1	0.901 ± 0.053	0.154 ± 0.016	42.0	1.419 ± 0.274
81.956 ± 0.184	2^-	43.3 ± 1.1	2.165 ± 0.120	0.278 ± 0.028	42.0	1.954 ± 0.352
82.758 ± 0.186	3^-	43.3 ± 1.1	0.486 ± 0.031	0.202 ± 0.057		
83.231 ± 0.188	2^-	43.3 ± 1.1	0.690 ± 0.048	0.188 ± 0.018		
83.829 ± 0.192	3^-	43.3 ± 1.1	1.109 ± 0.113	0.099 ± 0.018		
84.025 ± 0.195	2^-	43.3 ± 1.1	0.525 ± 0.158	0.140 ± 0.013		
84.552 ± 0.192	3^-	43.3 ± 1.1	2.171 ± 0.124	0.410 ± 0.038		
85.395 ± 0.198	3^-	43.3 ± 1.1	0.050 ± 0.015	0.502 ± 0.222		
86.461 ± 0.201	2^-	43.3 ± 1.1	0.376 ± 0.034	0.386 ± 0.090		
87.357 ± 0.203	3^-	43.3 ± 1.1	0.206 ± 0.022	0.060 ± 0.027		
87.836 ± 0.201	2^-	43.3 ± 1.1	5.102 ± 0.301	0.522 ± 0.047	42.0	4.880 ± 0.503
88.174 ± 0.205	3^-	43.3 ± 1.1	0.238 ± 0.047	0.495 ± 0.098		
89.215 ± 0.207	3^-	43.3 ± 1.1	0.612 ± 0.095	0.170 ± 0.029		
89.480 ± 0.206	2^-	43.3 ± 1.1	2.720 ± 0.191	0.201 ± 0.021	42.0	2.110 ± 0.364
91.934 ± 0.213	3^-	43.3 ± 1.1	0.156 ± 0.022	0.251 ± 0.105		
93.258 ± 0.215	3^-	43.3 ± 1.1	6.112 ± 0.383	0.128 ± 0.013	42.0	7.039 ± 0.504
94.448 ± 0.219	2^-	43.3 ± 1.1	1.154 ± 0.090	0.204 ± 0.036		
95.260 ± 0.221	3^-	43.3 ± 1.1	0.608 ± 0.093	0.131 ± 0.028		
95.556 ± 0.222	2^-	43.3 ± 1.1	3.890 ± 0.260	0.120 ± 0.013	42.0	3.854 ± 1.196
95.970 ± 0.223	3^-	43.3 ± 1.1	2.989 ± 0.192	0.156 ± 0.016	42.0	3.747 ± 1.564
96.328 ± 0.224	2^-	43.3 ± 1.1	3.753 ± 0.268	0.236 ± 0.025	42.0	4.954 ± 1.561
97.266 ± 0.226	3^-	43.3 ± 1.1	0.424 ± 0.039	0.294 ± 0.065		
98.174 ± 0.228	3^-	43.3 ± 1.1	0.380 ± 0.034	0.110 ± 0.057		
99.978 ± 0.225	2^-	43.3 ± 1.1	1.679 ± 0.115	0.140 ± 0.077		
101.420 ± 0.229	3^-	43.3 ± 1.1	2.922 ± 0.194	0.166 ± 0.020	42.0	3.116 ± 0.407
102.360 ± 0.238	2^-	43.3 ± 1.1	0.415 ± 0.065	0.218 ± 0.070		
103.020 ± 0.233	3^-	43.3 ± 1.1	6.980 ± 0.478	0.260 ± 0.027	42.0	7.898 ± 0.699
104.600 ± 0.238	3^-	43.3 ± 1.1	2.233 ± 0.154	0.157 ± 0.025		
105.960 ± 0.246	2^-	43.3 ± 1.1	10.281 ± 0.737	0.316 ± 0.034	42.0	15.318 ± 1.423
106.240 ± 0.247	3^-	43.3 ± 1.1	3.106 ± 0.307	0.482 ± 0.053	42.0	
107.420 ± 0.249	2^-	43.3 ± 1.1	2.867 ± 0.208	0.154 ± 0.020	42.0	
107.840 ± 0.250	2^-	43.3 ± 1.1	0.225 ± 0.058	0.176 ± 0.075		
109.050 ± 0.253	3^-	43.3 ± 1.1	0.121 ± 0.036	0.050 ± 0.022		

TABLE IV. (Continued.)

		This work			Lampoudis et al. [5]	
E_{λ_c} (eV)	J^π ($\hbar$)	$\Gamma_{\lambda\gamma_c}$ (meV)	$\Gamma_{\lambda n_c}$ (meV)	$\Gamma_{\lambda f_c}$ (meV)	$\Gamma_{\lambda\gamma_c}$ (meV)	$\Gamma_{\lambda n_c}$ (meV)
109.630 ± 0.255	3^-	43.3 ± 1.1	3.464 ± 0.311	0.282 ± 0.031		
109.900 ± 0.255	2^-	43.3 ± 1.1	4.482 ± 0.378	0.344 ± 0.040	42.0	4.712 ± 1.362
111.060 ± 0.258	3^-	43.3 ± 1.1	0.601 ± 0.077	0.268 ± 0.055	42.0	1.309 ± 0.941
111.430 ± 0.260	2^-	43.3 ± 1.1	6.525 ± 0.480	0.145 ± 0.016		
111.980 ± 0.260	3^-	43.3 ± 1.1	0.171 ± 0.063	0.293 ± 0.120		
112.560 ± 0.261	3^-	43.3 ± 1.1	0.366 ± 0.044	0.402 ± 0.085		
113.020 ± 0.262	2^-	43.3 ± 1.1	0.497 ± 0.093	0.174 ± 0.091		
113.690 ± 0.269	3^-	43.3 ± 1.1	1.739 ± 0.133	0.123 ± 0.019		
114.380 ± 0.266	2^-	43.3 ± 1.1	0.182 ± 0.054	0.400 ± 0.137		
114.870 ± 0.271	3^-	43.3 ± 1.1	1.734 ± 0.135	0.248 ± 0.031		
115.540 ± 0.268	2^-	43.3 ± 1.1	0.969 ± 0.123	0.122 ± 0.029		
116.180 ± 0.273	3^-	43.3 ± 1.1	2.770 ± 0.214	0.185 ± 0.025		
118.300 ± 0.089	3^-	43.3 ± 1.1	0.778 ± 0.077	0.296 ± 0.066		
119.600 ± 0.089	3^-	43.3 ± 1.1	2.122 ± 0.187	0.079 ± 0.013		
119.900 ± 0.089	3^-	43.3 ± 1.1	1.954 ± 0.203	0.179 ± 0.027		
121.750 ± 0.278	2^-	43.3 ± 1.1	4.507 ± 0.373	0.030 ± 0.015		
122.380 ± 0.284	3^-	43.3 ± 1.1	2.449 ± 0.261	0.070 ± 0.029		
122.490 ± 0.284	2^-	43.3 ± 1.1	1.854 ± 0.311	0.045 ± 0.024		
122.960 ± 0.286	2^-	43.3 ± 1.1	2.661 ± 0.316	0.108 ± 0.044		
123.140 ± 0.286	3^-	43.3 ± 1.1	1.809 ± 0.207	0.440 ± 0.075		
124.650 ± 0.223	2^-	43.3 ± 1.1	2.282 ± 0.209	0.091 ± 0.024		
125.200 ± 0.291	3^-	43.3 ± 1.1	0.207 ± 0.071	0.810 ± 0.115		
125.600 ± 0.292	3^-	43.3 ± 1.1	0.856 ± 0.097	0.201 ± 0.030		
126.140 ± 0.228	2^-	43.3 ± 1.1	2.755 ± 0.304	0.150 ± 0.025		
127.140 ± 0.295	3^-	43.3 ± 1.1	0.174 ± 0.044	0.200 ± 0.120		
127.680 ± 0.222	2^-	43.3 ± 1.1	2.312 ± 0.219	0.194 ± 0.035		
129.360 ± 0.300	3^-	43.3 ± 1.1	0.164 ± 0.047	0.300 ± 0.107		
130.470 ± 0.097	2^-	43.3 ± 1.1	1.750 ± 0.166	0.196 ± 0.031		
131.060 ± 0.098	3^-	43.3 ± 1.1	2.930 ± 0.246	0.153 ± 0.021		
131.910 ± 0.098	3^-	43.3 ± 1.1	0.775 ± 0.107	0.130 ± 0.029		
132.490 ± 0.099	2^-	43.3 ± 1.1	1.550 ± 0.178	0.131 ± 0.023		
133.400 ± 0.100	3^-	43.3 ± 1.1	1.830 ± 0.164	0.210 ± 0.031		
134.550 ± 0.100	2^-	43.3 ± 1.1	7.933 ± 0.794	0.222 ± 0.030		
134.820 ± 0.100	2^-	43.3 ± 1.1	3.433 ± 0.700	0.294 ± 0.040		
135.240 ± 0.101	3^-	43.3 ± 1.1	3.114 ± 0.305	0.203 ± 0.029		
136.160 ± 0.101	2^-	43.3 ± 1.1	7.915 ± 0.679	0.386 ± 0.051		
136.830 ± 0.102	3^-	43.3 ± 1.1	1.239 ± 0.157	0.208 ± 0.029		
137.340 ± 0.102	2^-	43.3 ± 1.1	2.129 ± 0.230	0.072 ± 0.019		
138.500 ± 0.103	3^-	43.3 ± 1.1	3.721 ± 0.327	0.226 ± 0.031		
139.670 ± 0.104	3^-	43.3 ± 1.1	1.129 ± 0.151	0.134 ± 0.028		
140.200 ± 0.104	2^-	43.3 ± 1.1	3.161 ± 0.296	0.089 ± 0.014		
140.840 ± 0.105	3^-	43.3 ± 1.1	1.312 ± 0.275	0.183 ± 0.026		
141.160 ± 0.105	2^-	43.3 ± 1.1	8.547 ± 0.798	0.166 ± 0.023		
142.790 ± 0.106	3^-	43.3 ± 1.1	0.258 ± 0.053	0.605 ± 0.196		
144.570 ± 0.108	2^-	43.3 ± 1.1	1.821 ± 0.192	0.132 ± 0.025		
145.080 ± 0.108	3^-	43.3 ± 1.1	0.294 ± 0.064	0.060 ± 0.026		
146.130 ± 0.109	2^-	43.3 ± 1.1	2.361 ± 0.235	0.105 ± 0.026		
147.690 ± 0.110	3^-	43.3 ± 1.1	10.096 ± 0.983	0.108 ± 0.016		
147.980 ± 0.110	3^-	43.3 ± 1.1	1.556 ± 0.404	0.111 ± 0.017		
148.840 ± 0.111	3^-	43.3 ± 1.1	3.972 ± 0.373	0.317 ± 0.046		

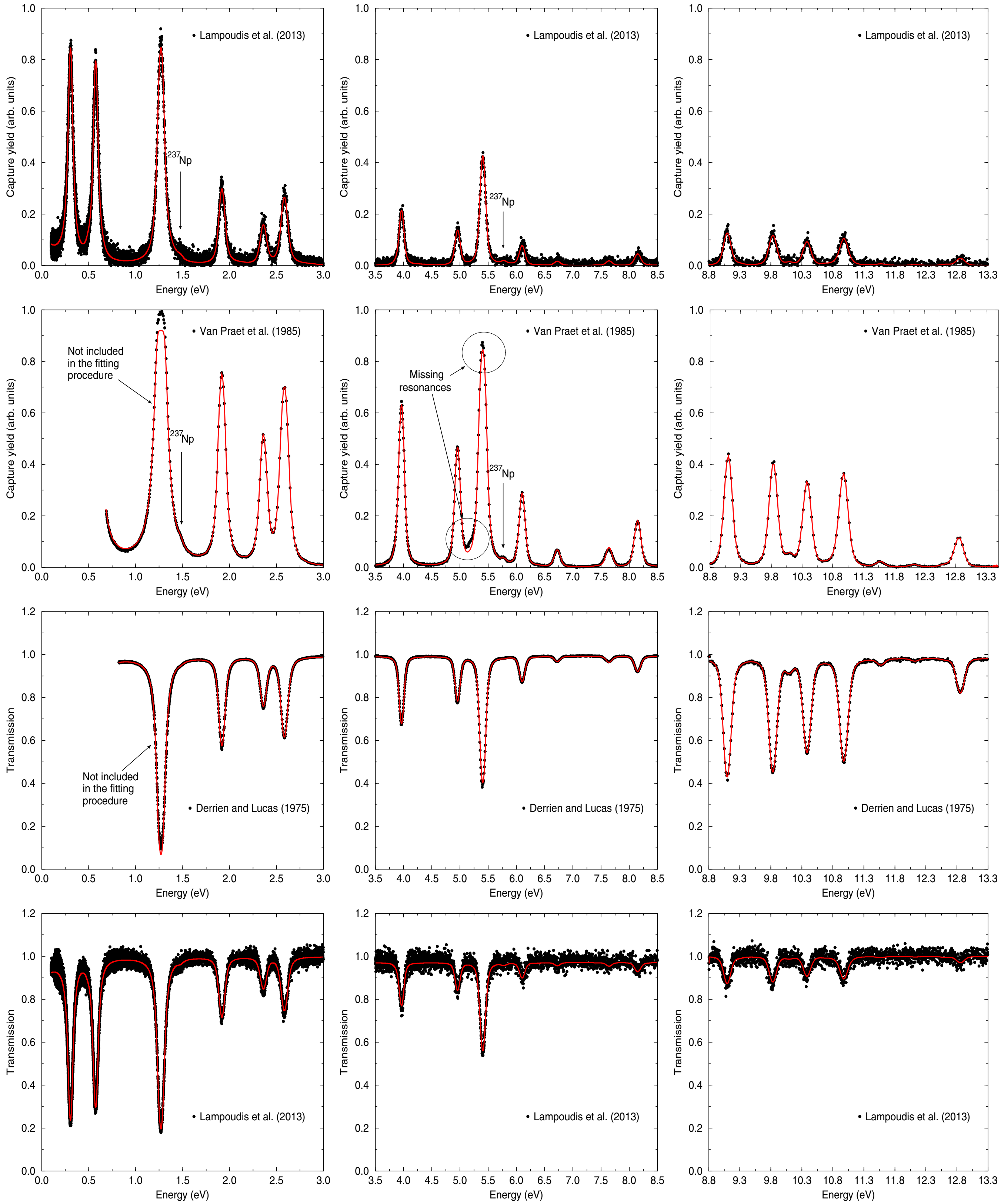

FIG. 6. (Color online) Theoretical capture yield and transmission calculated with the REFIT code up to 27 eV.

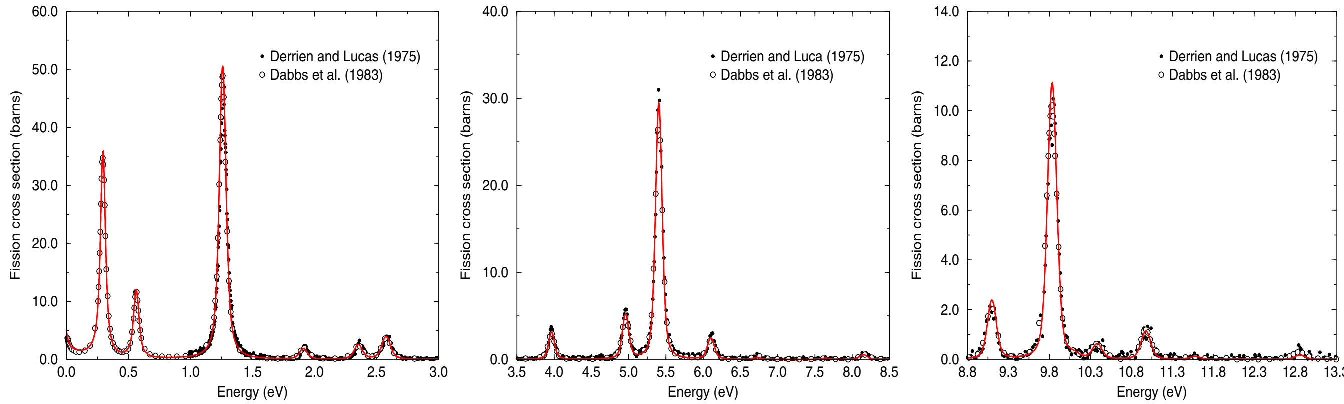

FIG. 7. (Color online) Theoretical fission cross section reconstructed up to 27 eV.

distribution obtained from the parameters in Table IV is given in Fig. 11 as a function of the threshold x which is defined as

$$x = \frac{g_J \Gamma^0_{n_J}}{\langle g_J \Gamma^0_{n_J} \rangle}. \tag{32}$$

At $x = 0$, the cumulative distribution is the number N_{exp} of experimentally observed resonances. A more rigorous estimate of the total number of s-wave resonance N_{th} can be derived from a least squares adjustment to the experimental cumulative distribution by varying the value of the threshold x to be representative of the actual experimental cutoff. Such a procedure also accounts for the number of missing levels $\Delta N = N_{\mathrm{th}} - N_{\mathrm{exp}}$. In the present analysis, we obtain

$$\langle \Gamma^0_{n_J} \rangle = (6.03 \pm 0.70) \times 10^{-5}\ \mathrm{eV},$$

and

$$D_0 = 0.60 \pm 0.01\ \mathrm{eV}.$$

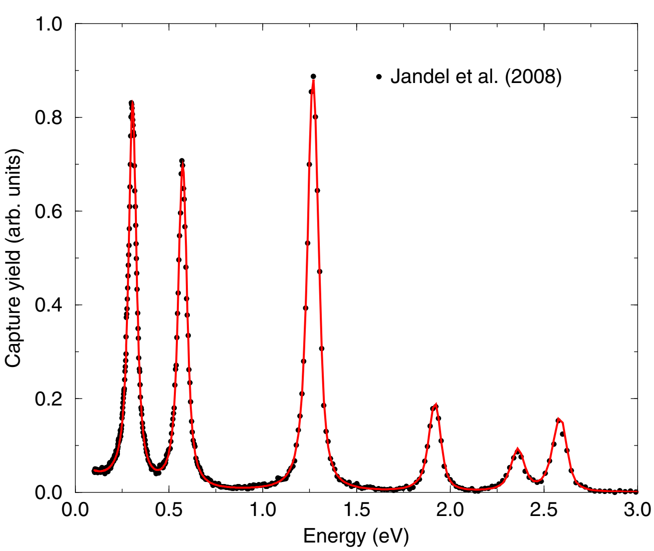

FIG. 8. (Color online) Capture yield calculated with the REFIT code compared to Jandel's data [6] up to 3 eV.

The neutron strength function is derived from the ratio of the reduced neutron width to the mean level spacing:

$$S_0 = (1.01 \pm 0.12) \times 10^{-4}.$$

The uncertainty on S_0 is obtained from the quadratic sum of the variances of D_0 and $\langle \Gamma^0_{n_J} \rangle$.

The estimates based on these values of S_0 and D_0 are shown in Fig. 11. The slope of the cumulative number of levels gives the level density $1/D_0$ and the slope of the cumulative $\Gamma^0_{n_J}$ values is a measure of the s-wave neutron strength function. This comparison shows the increasing number of missing resonances with neutron energy. The fraction of missing levels reaches $\sim$15% at 150 eV. The neutron strength function deduced from the ESTIMA method remains in good agreement with the trend observed from the staircase plot. These average resonance parameters are compared in Table V with those reported in the literature. Evidently there is a sound agreement obtained with the ones of Ref. [5]. The data in Table V suggest that the neutron strength function and mean level spacing in previous works [47,60] are underestimated.

C. Average *R*-matrix parameters established with the SPRT analysis

Among the average R-matrix parameters, we need to focus on the neutron strength function S_c and the distant level parameters R^∞_c in channel $c = \{l, J\}$. These parameters can be calculated from the matrix C_c provided by optical model calculations. The mathematical relationships are given by the Eqs. (16) and (17). These equations define the generalized SPRT method [13]. Historically, the acronym SPRT means s-wave neutron strength function (S), p-wave strength function (P), potential scattering radius (R), and neutron transmission coefficient (T). The original method was limited to $l = 0,1$. The generalized version allows calculation of average parameters for higher values of orbital momentum.

ECIS calculations were performed on the basis of the rigid rotor model using the optical model established by Soukhovitskii [44] and the parameters reported in the Japanese Evaluated Nuclear Data File of ^{241}Am. The latter are listed in Table VI. As proposed in Ref. [62], five ground-state rotational band levels ($5/2^-$, $7/2^-$, $9/2^-$, $11/2^-$ and $13/2^-$) were included in the coupled channel calculations. The deformation

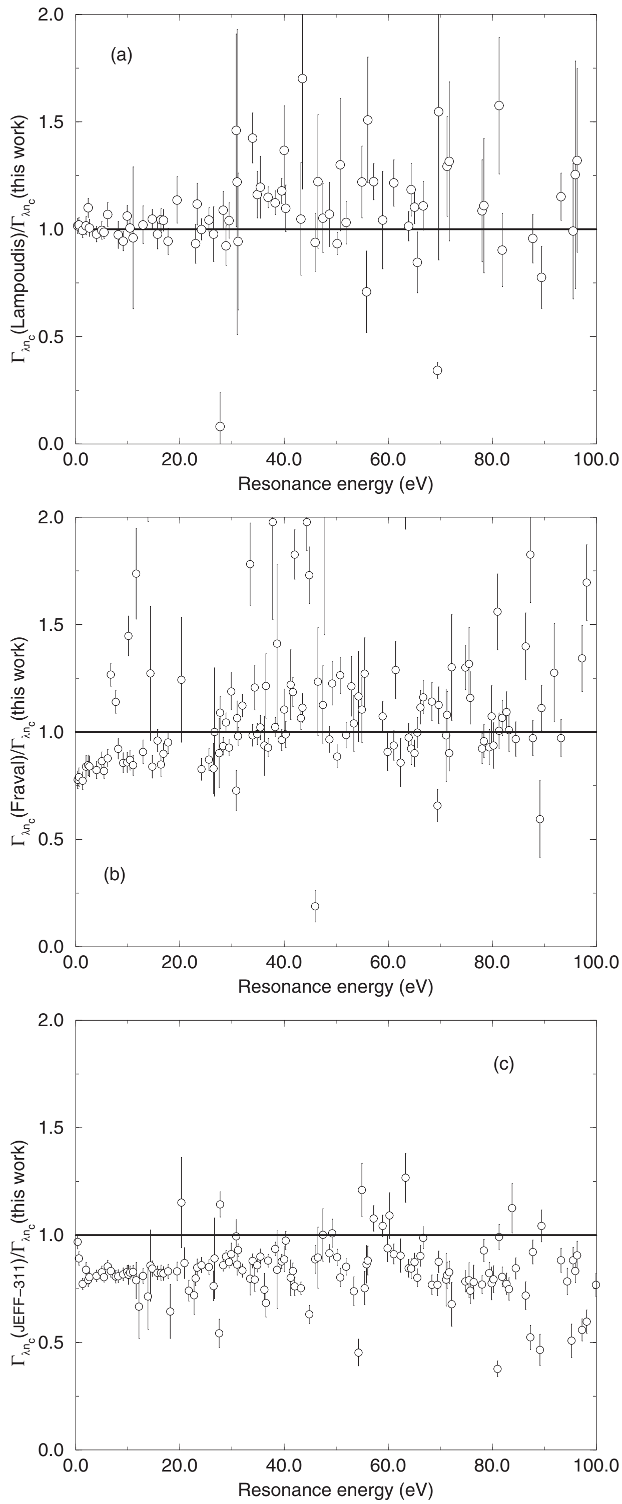

FIG. 9. Ratio of the neutron widths reported in Ref. [5] (a), in Ref. [59] (b), and compiled in the Evaluated Nuclear Data library JEFF-311 (c) to our results.

parameter β_2 was slightly optimized to improve the agreement with the S_0 value established with the ESTIMA method (Table V). Uncertainties and correlation matrix for the optical

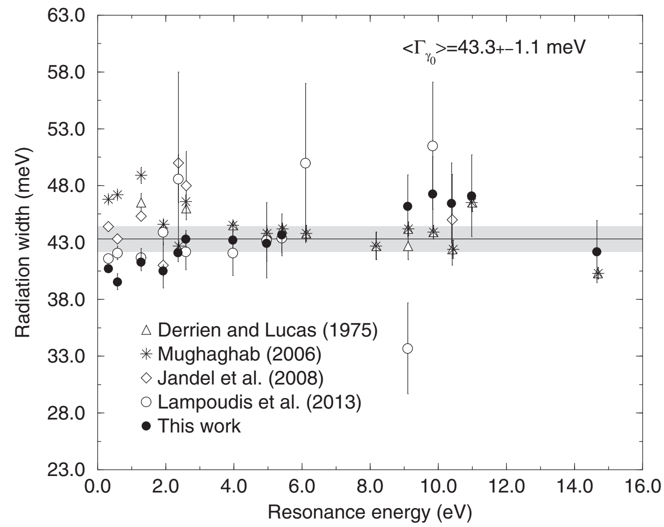

FIG. 10. Comparison of the individual radiation widths determined in the present work with results reported in the literature.

model parameters of interest for this work (geometrical parameters, depth of the potentials and deformation parameters) are given in Table VII. They were determined by propagating the uncertainties of the experimental total cross section of Philips and Howe [63] and the s-wave neutron strength function in Table V, using the conventional uncertainty propagation applied in least-squares adjustments. In Fig. 12, the total cross section calculated with ECIS is compared with the EXFOR data.

Figure 13 shows the neutron strength function S_l and the distant level parameter R_l^∞ obtained for the nuclear system ${}^{241}\mathrm{Am} + n$ by using the optical model parameters proposed in the evaluated nuclear data file JENDL-4 (Table VI) together with the slightly modified deformation parameter (Table VII). Two sets of S_l values were deduced from the SPRT equations by introducing the equivalent hard-sphere radii listed in Table I and the channel radius of the ENDF convention reported in Table II. A Lagrange polynomial interpolation was used to extrapolate the low energy behavior of S_l and R_l^∞. Results reported in Table VIII are given at the neutron binding energy.

As expected, non-negligible differences are obtained for p- and d-wave neutron strength functions. However, when the equivalent hard-sphere radii are used, the distant level parameter vanishes ($R_l^\infty \simeq 0$). Consequently, Eq. (8) indicates that the channel radius a_c becomes strictly equivalent to the potential scattering radius R'. As stated by Vogt in the 1990s, the equivalent hard-sphere radius becomes the "natural" choice of a_c for each reaction channel [41]. For s-wave channels, it represents the "effective" radius R' of the target at zero energy:

$$R' = 9.52 \pm 0.60 \text{ fm}.$$

For low values of orbital angular momentum l and distant level parameters R_c^∞, it is also of great interest to observe that the approximation proposed by Frohner [64],

$$R'_c \simeq a_c\left[1 - (2l + 1)R_c^\infty\right]^{1/(2l+1)}, \tag{33}$$

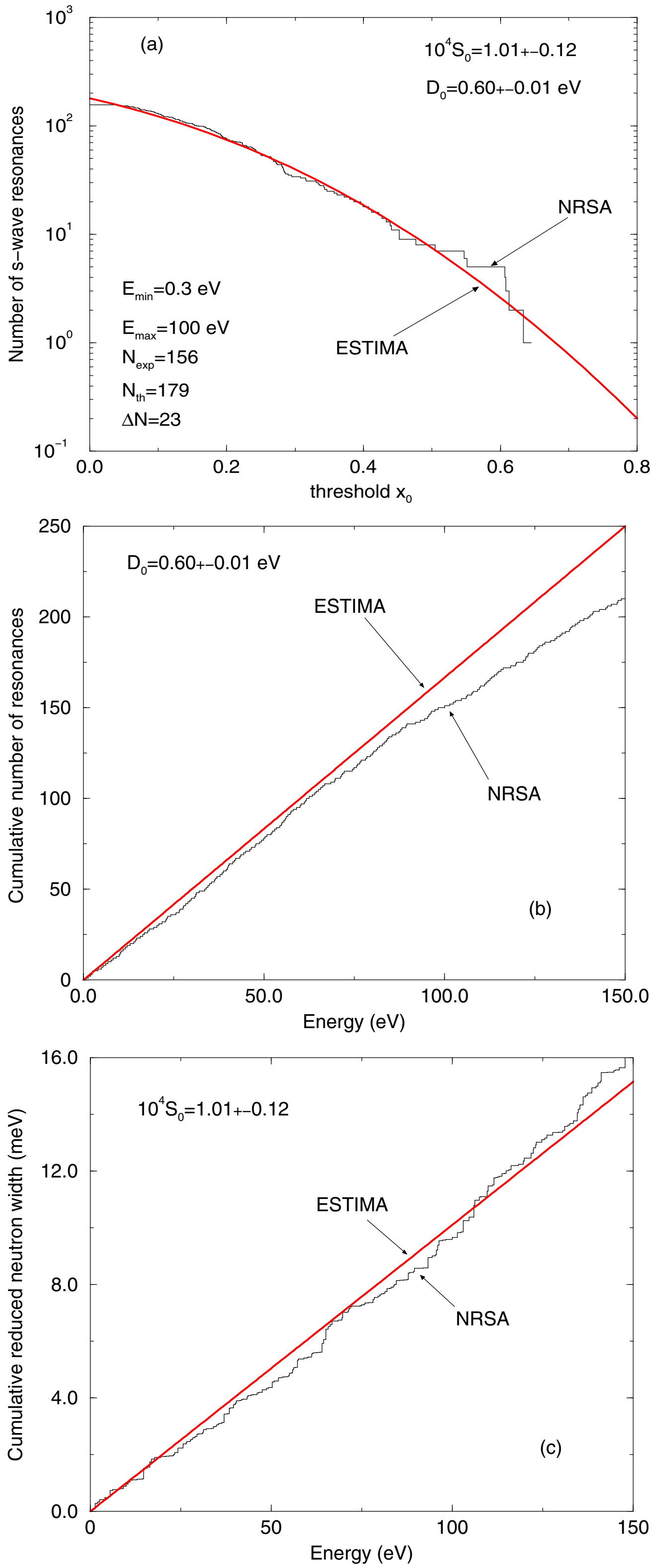

FIG. 11. (Color online) Comparisons of the ESTIMA calculations to the experimental distributions established from the neutron resonance shape analysis (NRSA). Plot (a) represents the cumulative Porter-Thomas integral distribution, plot (b) stands for the cumulative number of the s-wave resonances, and plot (c) is the cumulative distribution of the reduced neutron widths.

TABLE V. Average radiation width, mean level spacing and neutron strength function reported in the literature and found in this work from a statistical analysis of the resonance parameters reported in Table IV.

Author	Ref.	$\langle\Gamma_{\gamma 0}\rangle$ (meV)	D_0 (eV)	$10^4 S_0$
Derrien	[47]	43.77 ± 0.72	0.55 ± 0.05	0.94 ± 0.09
Mughaghab	[60]	45.0 ± 2.0	0.55 ± 0.05	0.90 ± 0.09
Lampoudis	[5]	42.1 ± 0.3	0.63 ± 0.11	0.98 ± 0.10
This work		43.3 ± 1.1	0.60 ± 0.01	1.01 ± 0.12

is able to provide similar values for R'_c within the ENDF convention or the equivalent hard-sphere approximation (Table IX).

The main conclusion is that the SPRT method yields s-wave and d-wave neutron strength functions of similar magnitude,

$$S_0 \simeq S_2,$$

if and only if the optical model and its equivalent square-well provide the same phase shifts at the common channel radii a_c. Additional calculations were performed to investigate the behavior of the neutron strength functions for $l = 3$ and $l = 4$. The equivalent hard-sphere approximation provides

$$S_3 = 2.51 \times 10^{-4},$$

and

$$S_4 = 1.06 \times 10^{-4},$$

TABLE VI. Optical model parameters reported in the Japanese Evaluated Nuclear Data File JENDL-4 for ^{241}Am.

Potential contribution	Parameter	Value
Volume potential	V_0	48 MeV
	λ_{HF}	0.004 1/MeV
	C_{viso}	15.9 MeV
	A_v	12.04 MeV
	B_v	81.36 MeV
	E_a	385 MeV
	r_v	1.255 fm
	a_v	0.58 fm
Surface potential	W_0	17.2 MeV
	B_s	11.19 MeV
	C_s	0.01361 1/MeV
	C_{wiso}	23.5 MeV
	r_s	1.15 fm
	a_s	0.601 fm
Spin-orbit potential	V_{so}	5.75 MeV
	λ_{so}	0.005 1/MeV
	W_{so}	−3.1 MeV
	B_{so}	160 MeV
	r_{so}	1.1214 fm
	a_{so}	0.59 fm
Deformation parameters	β_2	0.213
	β_4	0.08
	β_6	0.0015

TABLE VII. Optical model parameters, variance, and correlation matrix established in this work for the reduced radii (r_v, r_s), diffuseness (a_v, a_s), potential depths (V_0, A_v, W_0) and deformation parameters (β_2 and β_4).

Parameter	Value	Rel. unc.	Correlation matrix								
r_v (fm)	1.255 ± 0.045	(3.6%)	100								
a_v (fm)	0.580 ± 0.035	(6.0%)	−17	100							
V_0 (MeV)	48.0 ± 2.6	(5.4%)	−91	−8	100						
A_v (MeV)	12.04 ± 0.51	(4.2%)	−6	17	−5	100					
r_s (fm)	1.150 ± 0.019	(1.7%)	−88	−8	98	−9	100				
a_s (fm)	0.601 ± 0.036	(6.0%)	−17	100	−8	17	−8	100			
W_0 (MeV)	17.2 ± 0.9	(5.2%)	−6	6	−5	4	−9	6	100		
β_2	0.218 ± 0.013	(6.0%)	0	11	−35	16	−37	11	5	100	
β_4	0.080 ± 0.003	(3.8%)	43	−8	−37	−9	−37	−8	−1	−34	100

while the ENDF convention leads to $S_3 = 1.81 \times 10^{-4}$ and $S_4 = 1.15 \times 10^{-4}$. These results provide a mathematical framework for the "rule of thumb" often used by Fröhner and Bouland [65], which defines the behavior of the neutron strength functions for odd and even angular momentum l. For higher-order partial waves, this empirical rule says that the strength functions for $l = 0,2,4,\ldots$ are similar, and those for $l = 1,3,5,\ldots$ are likewise similar. Such low-energy neutron spectroscopic information could become a constraint in the optimization procedure of the optical model parameters.

D. Results and discussions

In the unresolved resonance range, the ^{241}Am(n,γ) reaction was calculated with the TALYS and CONRAD codes [66,67]. In both codes, the partial cross sections are calculated by means of the Hauser-Feshbach formula with width fluctuation correction factor [$W_{n\alpha_c}$ in Eq. (10)] using Moldauer's prescription.

The γ-ray transmission coefficient T_{γ_c} has an energy dependence carried by the Gilbert-Cameron level density formula [69] and giant dipole resonance (GDR) forms [70–72] whose parametrizations differ between the two codes. Such different GDR parametrizations have a limited impact over

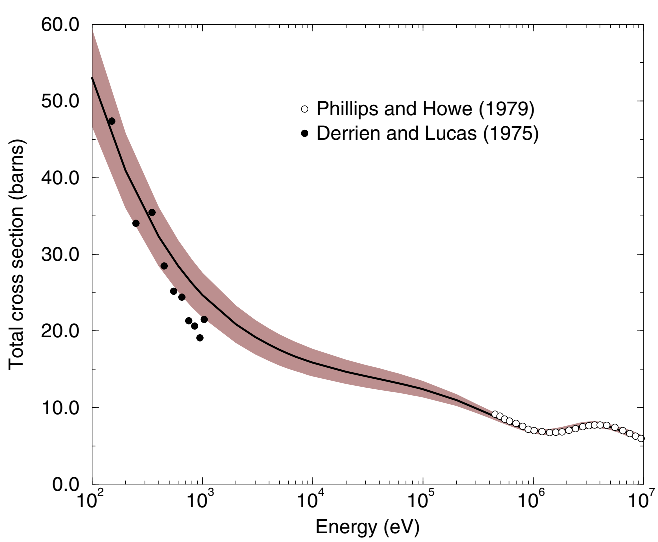

FIG. 12. (Color online) ^{241}Am total cross section obtained in this work (ECIS calculations) and compared with EXFOR data [47,63].

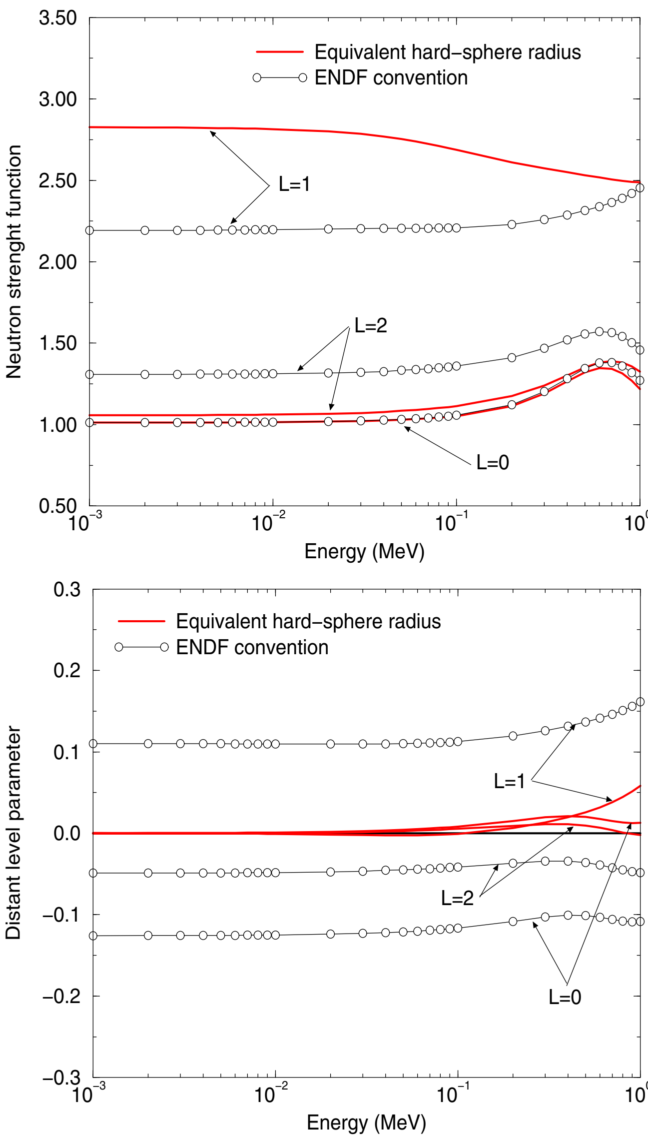

FIG. 13. (Color online) Neutron strength functions and distant level parameters obtained with the SPRT method [Eqs. (17) and (16)] for the nuclear system ^{241}Am + n. Channel radii calculated in the equivalent hard-sphere approximation and in the ENDF convention are reported in Tables I and II.

TABLE VIII. Neutron strength functions S_l and distant level parameter R_l^{∞} obtained with the SPRT method [Eqs. (16) and (17)] for the nuclear system ^{241}Am + n.

Parameters	ENDF convention	Equivalent hard-sphere
$10^4 S_0$	1.01 ± 0.12	1.01 ± 0.12
$10^4 S_1$	2.18 ± 0.33	2.82 ± 0.43
$10^4 S_2$	1.29 ± 0.29	1.06 ± 0.24
R_0^{∞}	−0.126 ± 0.071	≃0.0
R_1^{∞}	0.110 ± 0.028	≃0.0
R_2^{∞}	−0.049 ± 0.072	≃0.0

the unresolved resonance range because of the normalization of Eq. (11) performed for the s-wave channel:

$$\lim_{E\to 0} T_{\gamma_c}(E) = \frac{2\pi\langle\Gamma_{\gamma 0}\rangle}{D_0}, \tag{34}$$

in which $\langle\Gamma_{\gamma 0}\rangle$ and D_0 are provided by the statistical analysis of the resonance parameters (Secs. IV A and IV B). In order to calculate the neutron transmission coefficients from Eq. (12) the TALYS code uses the optical model code ECIS. The optical model parameters are listed in Tables VI and VII. The CONRAD code uses average resonance parameters established in Section IV C. The analytically averaged R-matrix expression (14) within the equivalent hard-sphere radius approximation ($R_c^{\infty} \simeq 0$) reduces to a simple expression for the neutron transmission coefficient:

$$T_{n_c} = \frac{2\pi S_c P_l \sqrt{E}}{P_0\left(1 + \frac{\pi S_c P_l \sqrt{E}}{2P_0}\right)^2}. \tag{35}$$

Figure 14 compares the neutron transmission coefficients provided by the ECIS code and calculated with Eq. (35) by using the neutron strength functions ($10^4 S_0 = 1.01$, $10^4 S_1 = 2.82$, $10^4 S_0 = 1.06$) and the equivalent hard-sphere radii ($a_0 = 9.52$ fm, $a_1 = 7.20$ fm, $a_2 = 8.76$ fm) reported in Table IX. A satisfactory agreement between the optical and average R-matrix models is observed up to 100 keV. The discrepancy remains below 5% and increases rapidly with the neutron energies. The larger difference is obtained for the p-wave channel. These results confirm that our parametrization of the average R-Matrix model can be applied over an energy range corresponding to the unresolved resonance range of the neutron cross sections.

The ^{241}Am capture cross section calculated with the TALYS code by using the mean level spacing ($D_0 = 0.6$ eV) and

TABLE IX. Comparison of the effective radii R'_l calculated with Eq. (33) by using a_l values established within the ENDF convention [Eq. (20)] and the equivalent hard-sphere approximation [Eq. (30)].

Parameters	ENDF convention	Equivalent hard-sphere
a_0 (fm)	8.46	9.52
a_1 (fm)	8.46	7.20
a_2 (fm)	8.46	8.76
R'_0 (fm)	9.52	9.52
R'_1 (fm)	7.40	7.20
R'_2 (fm)	8.82	8.76

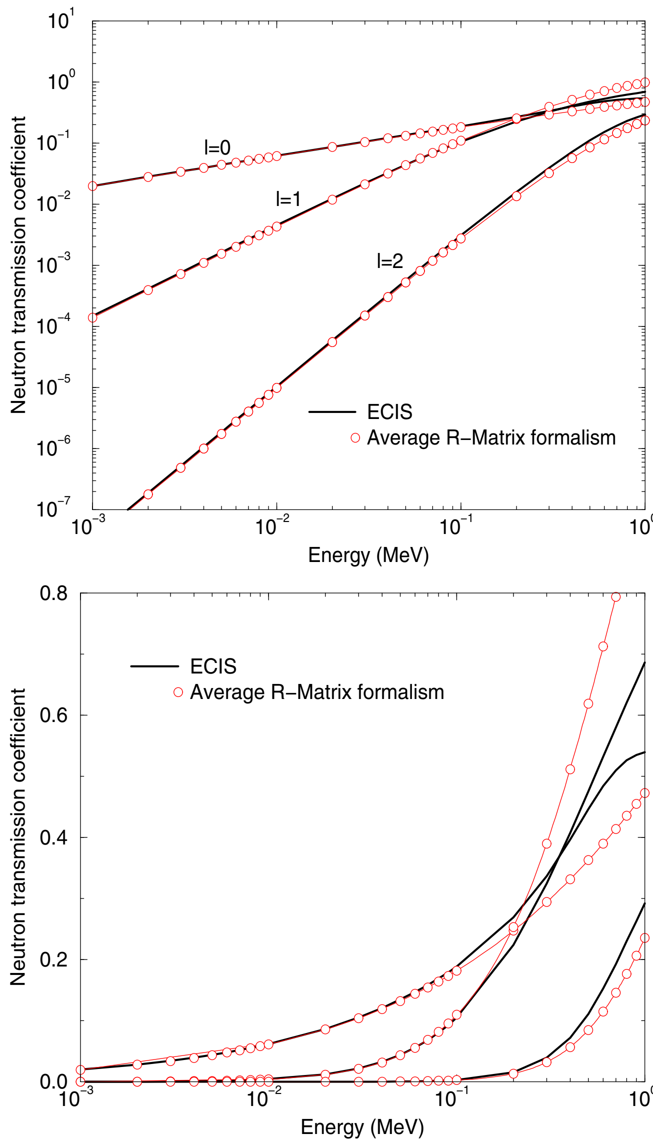

FIG. 14. (Color online) Comparison of the neutron transmission coefficients provided by the ECIS code and calculated with Eq. (35) for the nuclear system ^{241}Am + n in log-log and log-lin scales. The coupled channel calculations were performed with the optical model parameters listed in Tables VI and VII.

the average radiation width ($\langle\Gamma_{\gamma 0}\rangle = 43.3$ meV) reported in Table V is compared in Fig. 15 with data available in the EXFOR data base. Figure 16 shows the CONRAD cross sections for the s-, p-, and d-wave channels. The good agreement with the data and between the two codes confirms the partial-wave breakdown of the cross sections deduced from the statistical analysis of the resolved resonance parameters. The theoretical capture cross sections obtained in this work are reported in Table X up to 300 keV.

V. CONCLUSIONS

A consistent set of neutron resonance parameters for the nuclear system ^{241}Am + n was established up to 150 eV via

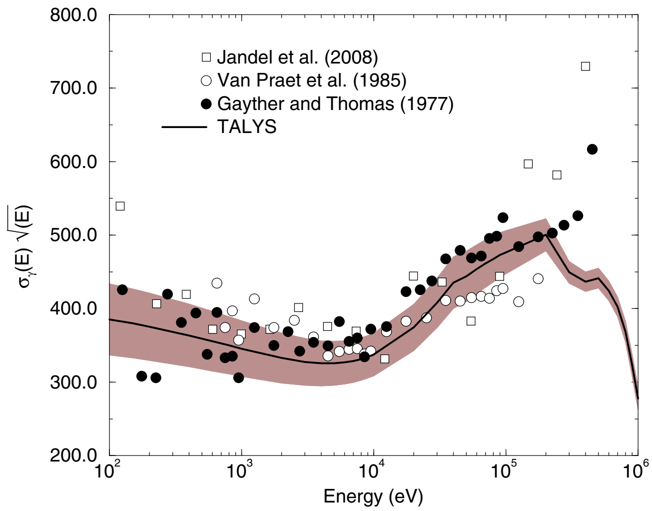

FIG. 15. (Color online) Comparison of the theoretical ^{241}Am capture cross section (TALYS) with data retrieved from the EXFOR data base [6,51,68] time the square root of the incident neutron energy. No normalization factors were applied to the data.

TABLE X. ^{241}Am total and capture cross section (in barns) calculated with the ECIS, TALYS and CONRAD codes below 300 keV.

Energy (keV)	Total cross section CONRAD	ECIS	Capture cross section CONRAD	TALYS
0.1	53.03	53.02 ± 6.81	38.52	38.54 ± 4.84
0.2	40.84	40.91 ± 5.15	26.53	26.55 ± 3.84
0.4	32.24	32.30 ± 3.98	18.14	18.17 ± 2.13
0.6	28.43	28.49 ± 3.45	14.49	14.52 ± 1.66
0.8	26.18	26.23 ± 3.14	12.34	12.37 ± 1.38
1.0	24.63	24.68 ± 2.93	10.89	10.93 ± 1.20
2.0	20.82	20.87 ± 2.40	7.40	7.44 ± 0.76
3.0	19.14	19.20 ± 2.16	5.94	5.98 ± 0.58
4.0	18.14	18.20 ± 2.02	5.12	5.15 ± 0.49
5.0	17.46	17.53 ± 1.92	4.56	4.60 ± 0.42
6.0	16.96	17.03 ± 1.84	4.17	4.22 ± 0.38
7.0	16.57	16.65 ± 1.79	3.88	3.93 ± 0.35
8.0	16.26	16.34 ± 1.74	3.65	3.70 ± 0.32
9.0	16.00	16.09 ± 1.69	3.47	3.52 ± 0.31
10.0	15.78	15.87 ± 1.66	3.32	3.38 ± 0.29
20.0	14.55	14.68 ± 1.45	2.59	2.65 ± 0.22
30.0	13.96	14.11 ± 1.33	2.31	2.35 ± 0.19
40.0	13.57	13.72 ± 1.25	2.14	2.18 ± 0.18
50.0	13.26	13.43 ± 1.19	1.95	1.98 ± 0.15
60.0	13.00	13.17 ± 1.14	1.82	1.85 ± 0.14
70.0	12.78	12.95 ± 1.09	1.72	1.74 ± 0.12
80.0	12.57	12.75 ± 1.04	1.63	1.65 ± 0.11
90.0	12.38	12.56 ± 1.00	1.56	1.58 ± 0.10
100.0	12.21	12.38 ± 0.97	1.49	1.51 ± 0.09
200.0	10.82	10.96 ± 0.71	1.09	1.12 ± 0.05
300.0	9.83	9.93 ± 0.56	0.86	0.82 ± 0.03

the neutron resonance shape analysis of transmission, capture yield, and fission data measured with the time-of-flight technique. Data retrieved from the experimental database EXFOR were normalized thanks to the recent measurements performed at the JRC-IRMM. The results confirm the sizable differences from previously reported values for the neutron widths of low energy resonances and the ^{241}Am(n,γ) cross section in the thermal energy region. Average R-matrix parameters (neutron strength function and distant level parameter) were determined by focusing our analysis on the conspicuous role of the channel radius a_c. This parameter is one of the boundary condition introduced in the R-matrix theory assuming an abrupt division of the configuration space. The resonance theory has some undesirable features of the square-well potential for which a_c is chosen more or less arbitrarily. The use of an equivalent hard-sphere radius, deduced from phase shifts provided by optical model calculations, shows that the contribution of the distant level parameter vanishes in the average R-matrix formalism. As a consequence, the effective radius R' and the channel radius a_0 for resonances having zero neutron orbital angular momentum ($l = 0$) are the same quantity. It must be emphasized that, for ^{241}Am $+ n$, this property leads to neutron strength functions of similar magnitude for odd ($l = 1,3,5,\dots$) and even ($l = 0,2,4,\dots$) angular momentum.

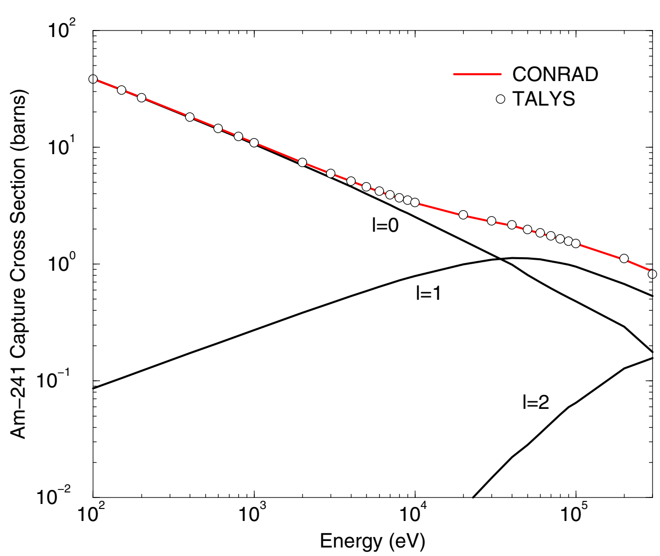

FIG. 16. (Color online) Comparison of the ^{241}Am capture cross section calculated with CONRAD and TALYS up to 300 keV.

In the present work, direct reactions are not taken into account throughout the analysis of the unresolved resonance parameters. Their contributions of few percent between 100 and 300 keV are lumped in the neutron transmission coefficients. A refined expression of the average R-matrix theory thanks to the reduced R-matrix established by Lynn would allow one to split the (l,J)-dependent neutron strength function in two components for the compound and direct reactions. This approach is under investigation for nonfissile deformed nuclei.

The study hereby represents a step forward to the change of paradigm recommended for the next generation of data evaluation. The latter involves in particular more consistency between the resonance range and neutron spectroscopy continuum. The new JEFF-3.2 evaluated data set for ^{241}Am is based on this model description.

ACKNOWLEDGMENTS

The authors wish to express his appreciation for the experimental work performed at the Institute for Reference Material and Measurements (IRMM, Belgium) in collaboration with the fundamental research institute IRFU of CEA/Saclay.

[1] M. C. Moxon and J. B. Brisland, REFIT computer code, Harwell Laboratory Report No. CBNM/ST/90-131/1, 1990 (unpublished).
[2] C. W. Reich and M. S. Moore, Phys. Rev. **111**, 929 (1958).
[3] A. M. Lane and R. G. Thomas, Rev. Mod. Phys. **30**, 257 (1958).
[4] H. Henriksson, O. Schwerer, D. Rochman, M. V. Mikhaylyukova, and N. Otuka, in *Proceedings of the International Conference on Nuclear Data for Science and Technology*, Nice, France, 2007, edited by O. Bersillon *et al.* (EDP Science, Les Ulis, 2008).
[5] C. Lampoudis, S. Kopecky, O. Bouland, F. Gunsing, G. Noguere, A. J. M. Plompen, C. Sage, P. Schillebeeckx, and R. Wynants, Eur. Phys. J. Plus **128**, 86 (2013).
[6] M. Jandel *et al.*, Phys. Rev. C **78**, 034609 (2008).
[7] S. Cathalau, R. Soule, and A. Benslimane, Some Remarks about the ^{241}Am Capture Cross-Sections and Branching Ratio, Nuclear Energy Agency Report No. JEFDOC-499, 1994 (unpublished).
[8] D. Bernard, O. Fabbris, and R. Gardet, Nucl. Sci. Eng. **179**, 302 (2015).
[9] F. Gunsing, A. Lepretre, C. Mounier, C. Raepsaet, A. Brusegan, and E. Macavero, Phys. Rev. C **61**, 054608 (2000).
[10] G. Noguere, O. Bouland, A. Brusegan, P. Schillebeeckx, P. Siegler, A. Lepretre, N. Herault, and G. Rudolf, Phys. Rev. C **74**, 054602 (2006).
[11] G. Noguere, Phys. Rev. C **81**, 044607 (2010).
[12] E. Fort and J. P. Doat, ESTIMA computer code, NEA Nuclear Data Committee Report No. NEANDC-161U, 1983 (unpublished).
[13] E. Rich, G. Noguere, C. De Saint Jean, and A. Tudora, Nucl. Sci. Eng. **162**, 76 (2009).
[14] P. A. Moldauer, ANL Report No. ANL/NDM-40, 1978 (unpublished).
[15] I. Sirakov, P. Schillebeeckx, and R. Capote, in Proceedings of the Workshop on Nuclear Data Evaluation for Reactor Applications, WONDER2006, Cadarache, France, 2006 (unpublished).
[16] I. Sirakov, R. Capote, F. Gunsing, P. Schillebeeckx, and A. Trkov, Ann. Nucl. Energy **35**, 1223 (2008); **36**, 131(E) (2009).
[17] I. Sirakov, B. Becker, R. Capote, E. Dupont, S. Kopecky, C. Massimi, and P. Schillebeeckx, Eur. Phys. J. A **49**, 144 (2013).
[18] R. E. MacFarlane and A. C. Kahler, Nucl. Data Sheets **111**, 2739 (2010).
[19] T. Teichmann and E. P. Wigner, Phys. Rev. **87**, 123 (1952).
[20] E. P. Wigner and L. Eisenbud, Phys. Rev. **72**, 29 (1947).
[21] J. E. Lynn, *The Theory of Neutron Resonance Reactions* (Clarendon Press, Oxford, 1968).
[22] H. Feshbach, C. E. Porter, and V. F. Weisskopf, Phys. Rev. **96**, 448 (1954).
[23] E. Vogt, Rev. Mod. Phys. **34**, 723 (1962).
[24] J. E. Lynn, Proc. Phys. Soc. **82**, 903 (1963).
[25] W. Hauser and H. Feshbach, Phys. Rev. **87**, 366 (1952).
[26] P. A. Moldauer, Phys. Rev. C **11**, 426 (1978).
[27] R. G. Thomas, Phys. Rev. **97**, 224 (1955).
[28] P. A. Moldauer, Phys. Rev. **129**, 754 (1963).
[29] F. C. Barker, Aust. J. Phys. **25**, 341 (1972).
[30] P. L. Kapur and R. Peierls, Proc. R. Soc. (Lond.) A **166**, 277 (1938).
[31] M. Herman, ENDF-102 Data Formats and Procedures for the Evaluated Nuclear Data File ENDF-6, Brookhaven National Laboratory Report No. BNL-NCS-44945-05-Rev, 2005 (unpublished).
[32] S. D. Drell, Phys. Rev. **100**, 97 (1955).
[33] W. D. Myers, Nucl. Phys. A **145**, 387 (1970).
[34] M. Bolsterli, E. O. Fiset, J. R. Nix, and J. L. Norton, Phys. Rev. C **5**, 1050 (1972).
[35] E. Vogt, *R*-Matrix Theory, *R*-Matrix School of the Joint Institute for Nuclear Astrophysics, Notre Dame University, Indiana, USA, 2004 (unpublished).
[36] P. E. Hodgson, Rep. Prog. Phys. **34**, 765 (1971).
[37] R. Capote *et al.*, Nucl. Data Sheets **110**, 3107 (2009).
[38] B. Morillon and P. Romain, Phys. Rev. C **70**, 014601 (2004).
[39] S. Hilaire and M. Girod, Eur. Phys. J. A **33**, 237 (2007).
[40] G. Michaud, L. Scherk, and E. Vogt, Phys. Rev. C **1**, 864 (1970).
[41] E. Vogt, Phys. Lett. B **389**, 637 (1996).
[42] F. H. Frohner, NEA/OECD report, JEFF Report No. 18 2000 (unpublished).
[43] J. Raynal, in *Proceedings of the Specialists' Meeting on the Nucleon Nucleus Optical Model up to 200 MeV*, Bruyeres-le-Chatel, France, 1996 (Nuclear Energy Agency, Paris, 1997).
[44] E. Sh. Soukhovitskii, R. Capote, J. M. Quesada, and S. Chiba, Phys. Rev. C **72**, 024604 (2005).
[45] B. Becker *et al.*, J. Instrum. **7**, 11002 (2012).
[46] F. Gunsing, P. Schillebeeckx, and V. Semkova, Summary Report of the Consultants' Meeting on EXFOR Data in Resonance Region and Spectrometer Response Function, IAEA Report No. INDC(NDS)-0647, 2013 (unpublished).
[47] H. Derrien and B. Lucas, *Proceedings of the Conference on Nuclear Cross Sections and Technology, Washington, US, 3-7 March 1975*, edited by R. A. Schrack and C.D. Bowman (NBS special publication, Washington, 1975), Vol II, p. 425.
[48] P. Schillebeeckx *et al.*, Nucl. Data Sheets **113**, 3054 (2012).
[49] B. Becker *et al.*, *Implementation of an Analytical Model Accounting for Sample Inhomogeneities in* REFIT, JRC Scientific and Policy Reports, JRC 86936 (Publications Office of the European Union, Luxembourg, 2013).
[50] B. Becker *et al.*, Eur. Phys. J. Plus **129**, 58 (2014).
[51] G. Vanpraet *et al.*, in Proceedings of the International Conference on Nuclear Data for Science and Technology, Santa Fe, 1986 (unpublished).
[52] J. W. T. Dabbs, C. H. Johnson, and C. E. Bemis, Nucl. Sci. Eng. **83**, 22 (1983).
[53] A. Brusegan, G. Noguere, and F. Gunsing, Nucl. Sci. Technol. Suppl. **2**, 685 (2002).
[54] C. De Saint Jean, G. Noguere, B. Habert, and B. Iooss, Nucl. Sci. Eng. **161**, 363 (2009).
[55] B. Becker, S. Kopecky, and P. Schillebeeckx, Nucl. Data Sheets **123**, 171 (2015).
[56] P. Schillebeeckx, B. Becker, R. Capote, F. Emiliani, K. Guber, J. Heyse, K. Kauwenberghs, S. Kopecky, C. Lampoudis, C. Massimi, W. Mondelaers, M. Moxon, G. Noguere, A. J. M. Plompen, V. Pronayev, P. Siegler, I. Sirakov, A. Trkov, V.

Volev, and G. Zerovnik, *Evaluation of Neutron Resonance Cross Section Data at GELINA*, special issue of Nucl. Data Sheets **119**, 94 (2014).

[57] P. Schillebeeckx, B. Becker, H. Harada, and S. Kopecky, in *Recent State of Art in Neutron Resonance Spectroscopy*, Landolt-Börnstein, New Series, Subvolume I/26A, Subseries: Elementary Particles, Nuclei and Atoms, Supplement to Subvolume B (Springer-Verlag, Berlin, 2015).

[58] A. Borella *et al.*, Nucl. Instrum. Methods A **577**, 626 (2007).

[59] K. Fraval *et al.*, Phys. Rev. C **89**, 044609 (2014).

[60] S. F. Mughabghab, *Atlas of Neutron Resonances*, 5th ed. (Elsevier, Amsterdam, 2006).

[61] C. E. Porter and R. G. Thomas, Phys. Rev. **104**, 483 (1956).

[62] P. Talou *et al.*, Nucl. Sci. Eng. **155**, 84 (2007).

[63] T. W. Phillips and R. E. Howe, Nucl. Sci. Eng. **69**, 375 (1979).

[64] F. H. Frohner, in Proceedings of the International Conference on Computation and Analysis of Nuclear Data Relevant to Nuclear Energy and Safety, Trieste, Italy, 1992 (unpublished); see also F. H. Frohner, Theory of Neutron Resonance Cross Sections for Safety Applications, Report No. KFK-5073, Karlsruhe Institute of Technology, 1992 (unpublished).

[65] F. H. Frohner and O. Bouland, Nucl. Sci. Eng. **137**, 70 (2001).

[66] A. J. Koning, S. Hilaire, and M. C. Duijvestijn, in *Proceedings of the International Conference on Nuclear Data for Science and Technology*, Santa Fe, New Mexico, 2004, edited by R. C. Haight *et al.* (American Institute of Physics, New York, 2005).

[67] C. De Saint Jean, B. Habert, O. Litaize, G. Noguere, and C. Suteau, in *Proceedings of the International Conference on Nuclear Data for Science and Technology*, Nice, France, 2007, edited by O. Bersillon *et al.* (EDP Science, Les Ulis, 2008).

[68] W. Gayther and B. W. Thomas, in Proceedings of the International Conference on Neutron Physics, Kiev, 1977 (unpublished).

[69] A. Gilbert and A. G. W. Cameron, Can. J. Phys. **43**, 1446 (1965).

[70] D. M. Brink, Oxford doctoral thesis, 1955 (unpublished).

[71] P. Axels, Phys. Rev. **126**, 671 (1962).

[72] J. Kopecky and M. Uhl, Phys. Rev. C **41**, 1941 (1990).